

Study of Mn *d-d* emission mechanisms in II-VI semiconductor nanocrystals

A thesis submitted in partial fulfillment for the degree of

MASTER OF SCIENCE

as a part of the

Integrated Ph.D Programme (Chemical Sciences)

by

Mr. Kushagra Gahlot



New Chemistry Unit

Jawaharlal Nehru Centre for Advanced Scientific Research

(A Deemed University)

Bangalore – 560064, India

March 2015

DECLARATION

I hereby declare that the matter embodied in the thesis entitled “**Study of Mn²⁺ *d-d* emission mechanisms in II-VI semiconductor nanocrystals**” is the result of investigations carried out by me at the New Chemistry Unit, Jawaharlal Nehru Centre for Advanced Scientific Research, Bangalore, India under the supervision of Dr. Ranjani Viswanatha and that it has not been submitted elsewhere for any degree or diploma.

In keeping with the general practice in reporting scientific observations, due acknowledgement has been made whenever the work described is based on the findings of other investigators. Any omission that might have occurred by oversight or error of judgment is regretted.

March 2015

Kushagra Gahlot



**Jawaharlal Nehru Centre for
Advanced Scientific Research**

Dr. Ranjani Viswanatha
New Chemistry Unit
Jawaharlal Nehru Centre for Advanced
Scientific Research (JNCASR)
Bangalore-560064,India
Phone : +91 80 2208 2573
E-mail: rv@jncasr.ac.in

Date:

March 31, 2015

CERTIFICATE

I hereby certify that the work described in this thesis titled “**Study of Mn²⁺ d-d emission mechanisms in II-VI semiconductor nanocrystals**” has been carried out by Mr. Kushagra Gahlot at the New Chemistry Unit, Jawaharlal Nehru Centre for Advanced Scientific Research, Bangalore, India under my supervision and it has not been submitted elsewhere for the award of any degree or diploma.

Dr. Ranjani Viswanatha

(Research Supervisor)

Dedicated to my Family

ACKNOWLEDGEMENTS

Firstly I would like to thank my research supervisor Dr. Ranjani Viswanatha for her constant guidance and support throughout the course of my research. I am very grateful to her for suggesting such an interesting project and encouraging me towards new explorations. I also acknowledge the academic freedom that I enjoyed in the lab.

I would also like to thank the Chairman of New Chemistry Unit, Prof. C. N. R. Rao, F.R.S., for being a source of constant inspiration. I am also thankful to him for providing necessary facilities to carry out this work.

I would like to thank all the faculties of NCU, CPMU and TSU for the various courses which were extremely helpful to me.

I express my sincere thanks to my senior lab mates Renu Tomar and Avijit Saha for their continuous help and support. Also it gives me great pleasure to thank all my past and present lab mates G. Krishnamurthy Grandhi, Amitha Shetty, Pavan Shagri, Pallabi Haldar and Mahima Makkar for many fruitful discussions that we had all through my research.

I am privileged to have wonderful batch mates, seniors and juniors. I thank them for all the help during my ups and downs in research life and also for their good friendship.

I would also like to thank Dr. Jay Ghatak, Sumit, Usha madam, Vasu and Anil for their help in characterization techniques. I thank all the academic, technical, library and complab staff at JNCASR.

I would also like to thank my college teachers, school teachers for their encouragement and blessings.

Finally I would like to thank my parents and younger brother for their encouragement, support and love.

PREFACE

This thesis entitled as “**Study of Mn *d-d* emission mechanisms in II-VI semiconductor nanocrystals**” is divided into three chapters:

Chapter 1 is the literature survey of all the research that has been pursued in the Mn doped nanocrystals exploring the challenges and rich physics involved in these type of Mn *d-d* emissions. Luminescence of Mn-doped semiconductor nanocrystals have been studied extensively over two decades but little is known about the dynamics of this atomic level forbidden Mn emission i.e. ${}^4T_1 \rightarrow {}^6A_1$. Mn doped II-VI nanocrystals shows intense emission and high efficiency as compared to the undoped nanocrystals. But specifically study of Mn luminescence in Mn doped CdSe has eluded most of the community that has been attributed to the crystal structure of CdSe nanocrystals.

Chapter 2 involves the study of the mechanism of Mn d-d emissions using CdSe and CdZnSe as host nanocrystals. We have systematically changed the band gap of the host nanocrystals by alloying Cd into ZnSe to study the mechanism of the Mn^{2+} Emission. This Cd alloying in the nanocrystals is done to bring the band edge levels close to the 4T_1 and 6A_1 state of the Mn^{2+} ion. The decay dynamics has been studied as a function of Cd incorporated in the Mn doped nanocrystals and it is evident that the host nanocrystals cannot be completely independent of Mn^{2+} emission as the band gap approached Mn^{2+} emission.

Chapter 3 involves the study of the mechanism of Mn d-d emissions in the presence of another optically active ion Ni^{2+} using CdS as host nanocrystals. Mn,Ni co-doped Cadmium Sulfide quantum dots (QDs) were synthesized using well established successive ion layer adsorption and reaction (SILAR) method. These transition metal ions will provide more than one impurity states within the band gap of the CdS nanocrystals which will affect the decay

dynamics of the excitons. This excitonic decay dynamics will show the contributions from both the optically active ions which have a difference in the lifetime of the order of some microseconds. Moreover, the relative position of the Ni²⁺ impurity level will be explored with respect to the Mn *d-d* levels and band edge levels of the host semiconductor nanocrystals. We studied their photo dynamics by varying the concentration ratio of Mn: Ni in the nanocrystals system.

CONTENTS

Declaration

Certificate

Acknowledgements

Preface

Contents

List of figures.....1

Chapter 1 Overview of Mn doped II-VI semiconductor nanocrystals.

1.1	Abstract.....	9
1.2	Introduction.....	10
1.2.1	Doping semiconductor nanocrystals.....	11
1.2.2	Transition metal doped semiconductor nanocrystals.....	12
1.2.3	Electronic structure of Mn ²⁺ ions.....	13
1.2.4	Mn doped systems : an overview.....	14
1.2.5	Co-doped nanocrystal systems.....	25
1.3	References and notes.....	27

Chapter 2 Study of Mn²⁺ *d-d* emission mechanism in CdSe and CdZnSe nanocrystals.

2.1	Abstract.....	33
2.2	Introduction.....	34
2.3	Experimental section.....	37
2.4	Characterizations and spectroscopic studies.....	41
2.5	Results and analysis.....	43
2.6	Discussions.....	65
2.7	Future work.....	66
2.8	References and notes.....	67

Chapter 3 Study of Mn²⁺ *d-d* emission mechanism in presence of other optically active ion (Ni²⁺).

3.1 Abstract.....	71
3.2 Introduction.....	72
3.3 Experimental section.....	75
3.4 Characterizations and spectroscopic studies.....	79
3.5 Results and discussions.....	81
3.6 Future work.....	91
3.7 References and notes.....	92

Chapter 1

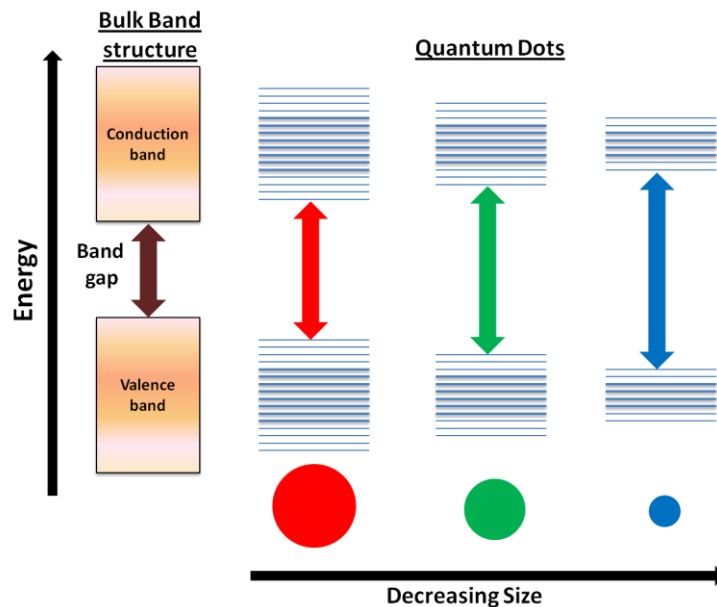
Overview of Mn doped II-VI semiconductor nanocrystals

1.1 Abstract

Doping of the nanocrystals with transition metal ion impurities like Mn, Cu, Ni etc can lead to various new types of nanomaterials having huge technological importance. The incorporation of impurities into the semiconductor lattices can significantly alter the optical, magnetic or other physical properties of the host nanocrystals. Luminescence of Mn-doped semiconductor nanocrystals have been studied extensively over two decades but little is known about the dynamics of this atomic level forbidden Mn emission i.e. ${}^4T_1 \rightarrow {}^6A_1$. Mn doped II-VI nanocrystals shows intense emission and high efficiency as compared to the undoped nanocrystals. But specifically study of Mn luminescence in Mn doped CdSe has eluded most of the community that has been attributed to the crystal structure of CdSe. In his chapter, there is a literature survey of all the research that has been pursued in Mn doped nanocrystals and the challenges that need to be taken for a better understanding of the dopant mechanism involved.

1.2 Introduction

With the advent of nanotechnology, many important fields have come up with the diverse applications in various interdisciplinary areas and indeed it has been observed that ‘there’s plenty of room at the bottom’ that was first quoted by the physicist Richard P. Feynmann. One of the most important scientific areas that have developed recently is Nanomaterials which ultimately lead to the emergence of nanotechnology. Nanomaterials show unique properties arising from their nanoscale dimensions. These special properties of the nanomaterials can be exploited to attain several useful applications. One such nanomaterial with huge potential are the Quantum Dots. These are tiny particles of the semiconducting material which confines the motion of conduction band electrons, valence band holes or excitons (bound pairs of conduction band electrons and valence band holes) in all three spatial directions.



Schematic 1.1 showing the size dependent band gap change as compared to bulk electronic structure

This confinement can be due to the electrostatic potentials (generated by the doping, strain, impurities), the presence of an interface between two semiconducting materials like core-shell nanocrystals system, the presence of semiconductor material surface like semiconductor nanocrystals or the combination of them. Schematic 1.1 shows the size dependent band gap change in quantum dots relative to the bulk. Thus, Quantum dot has a discrete quantized energy spectrum which shows size dependent optical properties.

1.2.1 Doping Semiconductor nanocrystals:

Bare Quantum dots have given rise to many practical problems at the commercial stage and so their properties need to be modified according to the usage. Doping of the colloidal semiconductor nanocrystals have led to various new advanced materials showing extraordinary potential for the commercial usage. The incorporation of impurities into semiconductor lattices alters the optical, magnetic and physical properties of the host semiconductor. Nanocrystals are synthesized by combining the molecular precursors containing the constituent elements. For doping, impurity containing precursor is added in the synthesis. So far colloidal synthesis methods have proven to be more versatile and easily processable than other methodologies. Doping in the bulk materials is very common now but extending it to semiconductor nanocrystals is not that trivial. This nanometer size regime leads to new difficulties that were not seen in the bulk materials. In heavily doped bulk semiconductor, we have about 1 dopant for every 10^5 atoms; a quantum dot with a 5 nm diameter has about a thousand atoms. Hence, to introduce a single impurity ion into each nanocrystal, the dopant level has to be increased by approximately 2 orders of magnitude. But just achieving this dopant level concentration doesn't solve the problem as the uniform distribution of the impurity atoms over the whole nanocrystals

does matters. Most of the times it has been observed that impurities remain on the surface of the nanocrystals mainly due to thermodynamic driving forces.

Most efforts to tackle these problems were mainly focused on doping II-VI semiconductor nanocrystals with the metals such as Mn^{1,3,7,8} or Cu^{1,9-11} and rare earth elements such as Eu^{12,13} or Tb¹⁴. These impurities don't influence the nanocrystals by introducing extra carriers but rather provides a new optically active pathway at the impurity center that interacts with quantum confined electron-hole pair. Though, these impurities don't affect the absorption spectra changes in the luminescence properties is clearly observed. Moreover, these impurities are paramagnetic in nature. These systems allow the study of spin-carrier or spin-spin interactions in the strongly quantum-confined regime making them strong contender for the applications in spintronics^{15,16}.

1.2.2 Transition metal doped Semiconductor nanocrystals:

Transition metal doping in the colloidal semiconductor nanocrystals have explored rich variety of properties i.e. high luminescence⁸, magneto-optical¹⁷, magneto-electronic¹⁸ etc which can be exploited for various applications¹⁹⁻²¹. These doped quantum dots shows number of advantages over undoped quantum dots which are large stokes shift minimizing self absorption, higher excited state lifetimes and robustness (thermal and environmental)^{7,8,11,22}. Various transition metal ions like Mn²⁺, Ni²⁺, Cu²⁺ etc were used as a dopant in the II-VI semiconductor nanocrystals^{1,2,9,22}. However, synthesis of these semiconductor nanocrystals is challenging so as to maintain the quality of the nanocrystals. The synthetic process used must lead to the high crystallinity, well-controlled size and uniform size distribution. These II-VI and III-V semiconductor nanocrystals doped with the different transition metal ions shows very stable, intense and tunable dopant emissions apart from the size tunable emission of the host

nanocrystals. The luminescence properties of transition metals specifically Mn^{2+} is interesting mainly due to forbidden nature of this transition. Hence, there is a need to understand the basic electronic structure of the dopant ion with respect to the host nanocrystals.

1.2.3 Electronic structure of Mn^{2+} ions:

The local electronic structure of Mn^{2+} ions in II-VI semiconductor nanocrystals is described well with the help of Ligand field theory. Mn^{2+} ion has five $3d$ electrons having a singlet ground state with 6-fold spin degeneracy (6S). In the weak tetrahedral ligand fields, the ground state remains totally symmetric i.e. 6A_1 . The splitting of the degenerate $3d$ orbitals occurs into t_2 and e , two sets of orbitals. The lowest energy ligand field excited state in weak cubic fields is the 4T_1 state, which further splits by spin-orbit and Jahn teller interactions.

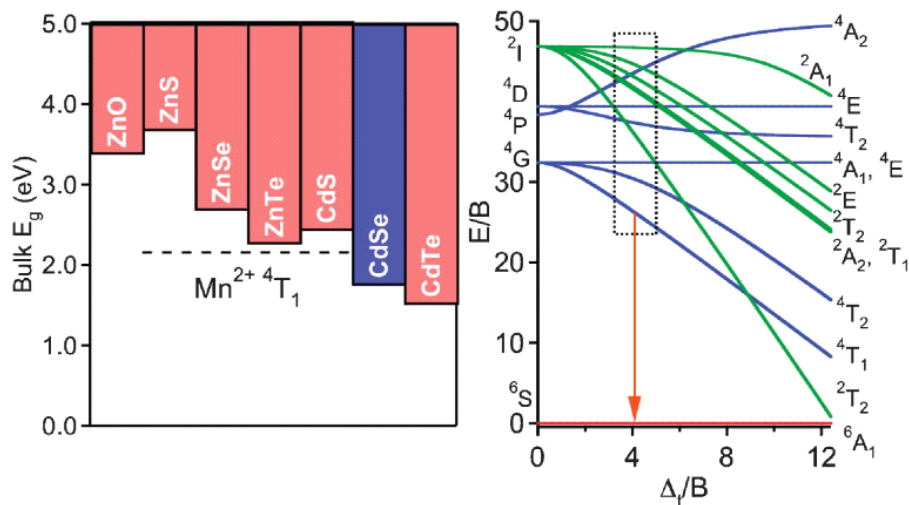


Figure 1.1 (reproduced from the reference²³) shows the relative bulk band gap with respect to 4T_1 state of Mn^{2+} ion. Tanabe Sugano diagram of Mn^{2+} ion in tetrahedral field.

Figure 1.1 shows the relative position of the 4T_1 state according to the bulk energy gaps and Tanabe Sugano diagram of Mn^{2+} ion in a cubic ligand field showing several spin forbidden ligand field states as well.

Here ${}^4T_1 \rightarrow {}^6A_1$ ligand field transition as shown by red arrow in figure 1.1 is responsible for the characteristic luminescence of Mn^{2+} ions in doped II-VI semiconductor nanocrystals. This ligand field transition is spin forbidden but is partially overcome by the spin-orbit coupling at the Mn^{2+} ion. If the concentration of Mn^{2+} ion is increased above a certain level, Mn^{2+} - Mn^{2+} exchange interactions also hampers the Mn emission which assists in the spin forbiddenness of the system⁸. The value of absorption coefficients is as low as 10^0 - 10^1 $M^{-1}cm^{-1}$ at the maxima for the ${}^6A_1 \rightarrow {}^4T_1$ transition compared with 10^5 - 10^6 $M^{-1}cm^{-1}$ for the first absorption maxima of typical direct-band gap semiconductor quantum dots. Therefore, these ligand field transitions are rarely observed in the absorption spectra of Mn^{2+} doped nanocrystals.

1.2.4 Mn doped Systems: an Overview

Doping of Mn ions has been widely studied in all kinds of semiconductor nanocrystals. There are vast number of literature reports on the different synthetic procedures, doping methods and precursors that have been used for the Mn^{2+} ion doping in several host nanocrystals. As already discussed in the electronic structure of Mn^{2+} ion, which has two ligand field states i.e. 6A_1 ground state and 4T_1 excited state corresponding to which these ions show the characteristic luminescence at 2.12 eV (~580 nm). This is the atomic like transition which occurs through the manganese ions and is independent of the host nanocrystals^{4,7,8}. As these Mn levels remains independent of the host nanocrystals either a change of the host using different elements or its band gap with size should not affect the Mn^{2+} emission.

One of the earliest reports that described the Mn^{2+} doping in nanocrystals came in 1994 by Bhargava *et al.*³ which showed for the first time that the doped semiconductor nanocrystals can yield both high luminescent efficiencies and lifetime shortening at the same time. The explanation of these observations were given on the basis of the interaction of *sp* electron hole of the host (ZnS) and the *d* electrons of the impurity (Mn) which belong to first category. These results have suggested that the doped nanocrystals are indeed a new class of materials which were unknown before. Although this explanation and observation has later proven wrong by several other works^{24,25} and it is now known that Mn^{2+} emission has a lifetime in milliseconds^{24,26}.

Mn^{2+} doped nanocrystals have been developed over time but the qualitative improvement remained stagnant for some time until Norris *et al.*⁷ have shown the synthesis of the high quality Manganese-doped ZnSe nanocrystals using dimethyl manganese as a dopant source. These doped nanocrystals were formed by the hot injection method. Luminescence, magnetic circular dichroism (MCD) and electron paramagnetic resonance (EPR) measurements were performed to confirm that the Mn impurities are embedded inside the nanocrystals. Here they have got nearly monodisperse, highly fluorescent, crystalline quantum dots that can be systematically prepared as a function of size. The luminescence spectra showed two peaks, one at 3.171 eV corresponding to the band edge and other at 2.138 eV corresponding to the Mn^{2+} emission. The band edge peak shown was more intense than the dopant peak. Although high quality Mn doped ZnSe nanocrystals were obtained but many questions remained unanswered as whether a single Mn-doped nanocrystals can emit from both the lowest electron-hole pair state and the internal Mn transition or there are two different species doped and undoped that are present and emitting at the same time. After this report, there has been an inflow of lots of literature over doping of

Mn²⁺ ions over a decade which has led to immense development in the synthetic strategies, new precursors and various new types of dopant materials. These new synthetic strategies have improved the quality of the doped nanocrystals to a much larger extent and provided a more insight into the emission mechanisms of these Mn doped nanocrystals.

Nag *et al.*²⁷ showed the synthesis of water soluble Mn²⁺ doped CdS nanocrystals in which for the first time it was became possible to obtain a distinct Mn²⁺ *d*-related emission well separated from the defect state emissions. They have systematically varied the reaction temperature to come to the optimum value where the Mn²⁺ *d*-emission was maximum. Exciting the samples with energies lower than the band gap energies of host nanocrystals but higher than the Mn²⁺ *d-d* transition energy doesn't give rise to any measurable PL intensity, proving that the Mn²⁺ *d-d* transition takes place following the energy transfer from CdS host nanocrystals to the dopant site. Following this work, same group²⁸ also reported the generation of white light from Mn²⁺ doped CdS nanocrystals for the first time by suitably tuning the relative surface-state emissions of the nanocrystal host and dopant emission. These nanocrystals exhibited a huge stokes shift, thus minimizing the problem of self absorption. There is still a shortcoming in the quality of nanocrystals produced and hence new synthetic techniques with different doping strategies need to be developed to tackle this problem. New type of doping strategy, nucleation-doping was successfully used by Pradhan *et al.*⁸ to show the formation of Mn doped ZnSe nanocrystals and also optimized this process using greener approaches. These doped dots showed high photoluminescence (~50%) quantum yield achieved by the controlled formation of small-sized MnSe nanoclusters as the core and a diffused interface between the nanocluster core and the ZnSe overcoating layers. These doped dots were found to be thermally stable²⁹. This

advancement in the synthetic chemistry of the doped nanocrystals improved the quality of the nanocrystals to a major extent.

In all the above mentioned reports^{6,22}, it has been observed that CdSe nanocrystals have proven difficult to dope. This has been attributed to the Zinc blende structure that is thought to facilitate dopant incorporation compared to wurtzite. Since CdSe normally crystallizes in wurtzite structure, it was thought to be difficult to dope. Thus in general, doping problem seems to be more acute in case of wurtzite nanocrystals. Nag *et al.*⁴ have achieved for the first time as high as ~7.5% Mn²⁺ doping in a wurtzite alloyed Zn_xCd_{1-x}S nanocrystals system. This doping percentage was much higher than the earlier reports even for nanocrystals host with the zinc blende structure. This synthetic approach opens up new route to dope the nanocrystals to macroscopic extent for the various applications. These studies⁴ have shown that the quantum efficiency per Mn²⁺ ion decreases exponentially with the average number of Mn²⁺ ions per nanocrystals. Several reports have come up in the recent years but mainly focused on the synthetic procedure problems and doping different host nanocrystals with manganese ions to improve the emission quality.

One of the rare cases in which Mn is doped in the wide gap semiconductor but Mn characteristic peak is not observed. This happens in Mn doped ZnO. Doping Mn into the bulk ZnO matrix offers an interesting way to alter various properties as in the band gap of the host material can be tuned from 3.3 eV to 3.7eV. This also changes the emission properties by providing an efficient channel for the recombination of the electron and hole via the Mn dopant d-levels. Studies on different Mn doped Quantum dots have revealed that the properties of these doped samples are influenced by the quantum confinement of electronic states. Thus, the properties of the doped nanocrystals are interesting as compared to the bulk.

Amongst the transition metal dopant ions, Co^{2+} and Ni^{2+} were first doped in free standing ZnO nanocrystals³⁰. Thereafter, Viswanatha *et al.*³¹ reported for the first time the synthesis and characterization of Mn-doped free standing ZnO nanocrystals with a particle size of few nanometers. They were able to obtain smaller particles and a good control over the size using the capping agent i.e. polyvinylpyrrolidone (PVP). The absorption properties of PVP-capped Mn doped ZnO exhibited an interesting variation of the band gap with the concentration of Mn. Fluorescence emission, Electron paramagnetic resonance (EPR) and X-ray absorption spectroscopy (XAS) provide evidence for the presence of Mn in the interior as well as on the surface of the nanocrystals. But these Mn doped ZnO nanocrystals have not shown the characteristic ${}^4\text{T}_1$ to ${}^6\text{A}_1$ transition showing that host nanocrystals must have introduced some states in between which are providing the other relaxation pathways. Later Wang *et al.*³² have also doped different transition metal ions in ZnO nanocrystals including Mn^{2+} following different synthetic strategy and got similar results. Various reports have come till now on Mn doped ZnO nanocrystals^{17,32-34}, but nobody has observed the characteristic Mn peak in these nanocrystals instead they have proved the presence of manganese using EPR and other techniques. Thus, the appearance of the lowest energy excited state within the semiconductor band gap makes the electronic structure and photophysical properties of Mn doped ZnO nanocrystals qualitatively different than other II-VI nanocrystals.

Doping the most studied transition metal dopant i.e. Mn^{2+} into the most studied semiconductor nanocrystals i.e. CdSe has remained a challenging task and belongs to the third category. As we look into the electronic structure of Mn^{2+} ion and the bulk band gap energy of CdSe nanocrystals, it becomes evident that the conduction band of CdSe and ${}^4\text{T}_1$ ligand field excited state of Mn^{2+} ion are quite close to each other. Once the bound exciton energy of the host

nanocrystals is transferred to the Mn 6A_1 state, one of the electrons inverts its spin, and changes to the excited 4T_1 state. Few Literature reports³⁵⁻³⁹ have proved that they were successful in doping Mn²⁺ ion in CdSe nanocrystals using different synthetic methods and precursors but only one report stands out from Bawendi *et al.*³⁵ which shows the use of the single source manganese and chalcogen-containing organometallic complex $Mn_2(\mu-SeMe)_2(CO)_8$ to prepare $Cd_{1-x}Mn_xSe$ quantum dots of various sizes. They mentioned simpler precursors containing only manganese were ineffective dopants when incorporated into the trioctylphosphine oxide (TOPO) method for making CdSe QDs. Extensive surface ligand exchange was performed to ensure that their quantitative measurements detected only manganese ions incorporated into the lattice, rather than loosely bound to the nanocrystals surface. Quantitative Electron paramagnetic resonance (EPR) and Wavelength dispersive x-ray spectroscopy (WDS) measurements on manganese-doped dots were in agreement. They have achieved dopant levels of ~ 1 Mn atom per QD reproducibly. Both a simple etching experiment and EPR hyperfine splitting show that the Mn dopant is distributed mainly near the surface of the CdSe lattice. The ${}^{113}Cd$ solid state NMR experiments revealed a much smaller T_1 relaxation time and a paramagnetic shift in the doped samples, consistent with manganese having substituted somewhere inside the nanocrystal lattice. Optical measurements show that doped QDs behave like undoped QDs in an external magnetic field, the behavior is consistent with the presence of an exchange field that is due to the interaction of the electron/hole spin with the paramagnetic impurity. Fluorescence line narrowing (FLN) spectra and Photoluminescence excitation (PLE) spectra of doped CdSe QDs provide new spectroscopic information which was previously unobserved but theoretically predicted, fine structure state. Every possible technique have been used in this paper to prove Mn doped CdSe nanocrystals but simpler Photoluminescence and lifetime studies have not revealed anything.

Many concepts on the difficulty of doping CdSe with Mn impurities have come up considering various aspects of synthesis and components involved in them. In 2005, Erwin *et al.*⁶ attributed this difficulty to “self-purification process”, an allegedly intrinsic mechanism whereby impurities are expelled. They have shown that the underlying mechanism that controls doping is the initial adsorption of impurities on the nanocrystals surface during growth. This depends on three main factors: Surface morphology, nanocrystals shape and surfactants in the growth solution. Literature survey revealed that all of the nanocrystals that have been successfully doped with individual Mn atoms (ZnS,ZnSe,CdS) exhibit the zinc blende structure. In contrast those that have wurtzite (CdSe) or rock-salt structure (PbS, PbSe) have either not been doped, or have required polychalcogenide precursors to incorporate Mn. They have shown that the binding energy of Mn on the (0001) surface of wurtzite CdSe is two times smaller than ZnSe (001) which suggested that previous failure to dope CdSe may have resulted not only from intrinsic properties of CdSe but also from parasitic binding of Mn by strong surfactants. Thus doping previously undopable wurtzite CdSe nanocrystals may be feasible, although it may be more difficult than ZnSe. Later, Nag *et al.*⁴ have shown for the first time as high as ~7.5% Mn²⁺ doping in a wurtzite alloyed Zn_xCd_{1-x}S nanocrystals system. Dalpian and Chelikowsky⁴⁰ have addressed this problem theoretically and came to conclusion that self purification is the main reason as to why it is difficult to synthesize this system. In nanocrystals, since the distance the defect or impurity has to travel to reach the surface is very small and it can easily leach out. Mn doped CdSe nanocrystals have been taken as a model system in this paper. They have explained their work using energetic arguments and have shown self purification as an intrinsic property of defects in semiconductor nanocrystals. They have found that the formation energies of defect increase as

the size of the nanocrystals decreases. Hence, this report claims that it is difficult to dope smaller nanocrystals.

To explain this anomaly of Mn doped CdSe nanocrystals, Du *et al.*⁴¹ have come up with a trapped dopant model which focuses onto the role of surfactants in the nanocrystals synthesis. For example, when the surfactant tetradecylphosphonic acid (TDPA) was used in the synthesis of CdSe nanocrystals attempts to dope the nanocrystals with Mn impurities failed but when hexadecyl amine (HDA) was used successful doping by Mn was demonstrated. Surfactant molecules can form chemical bonds not only to the nanocrystals but also to the impurity atoms in the solution which is more probable if the impurity and host atoms have same chemical valence. For example, in case of Mn doped CdSe QDs, both Cd and Mn are divalent. Hence a surfactant forms chemical bonds to surface Cd atoms will be likely also to bind Mn atoms. So if a surfactant molecule strongly binds impurity atoms, then doping will be hindered because the adsorption of impurities on the nanocrystals surface is preempted. Thus to doped CdSe QDs with Mn impurities, either force the nanocrystals to grow in Zinc blende structure or to switch to the surfactant that is weakly binding like HDA. However, inspite of all these theoretical predictions and models, Gamelin group^{38,39} claims to have successfully doped Mn impurities in CdSe QDs and have proposed the mechanism of decay based on their results.

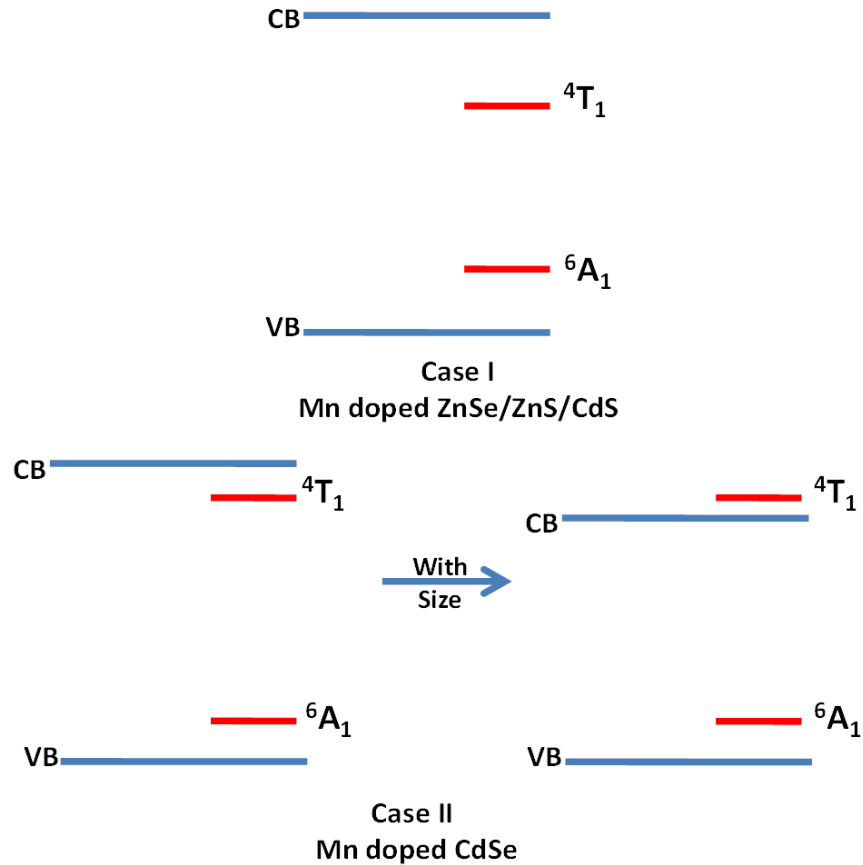
Recently, Hazarika *et al.*⁵ have developed a new class of manganese doped quantum dot materials where strain is used to tune the wavelength of the dopant emission , extending otherwise limited emission tunability over the yellow-orange range for manganese ions to almost the entire visible spectrum covering all colors from blue to red using ZnSe/CdSe/ZnSe core shell quantum dots. This impossible target of tuning the Mn emission has been achieved by controlling the strain generated due to an epitaxial growth of a semiconductor shell over a

semiconductor core. This result is important as such dopant emission bands were thought to have very limited tunability due to their essentially atomic nature. These synthetic chemistry advancements have just lead to the high quality doped nanocrystals. But not much has been studied about the decay dynamics of involving the band edge and Mn^{2+} levels. These were the difficulties one has to tackle to synthesize the Mn doped CdSe nanocrystals but understanding the way electronic structure is behaving in this host will give better insight into the processes taking place.

Following this series of thoughts, we can have two types of host nanocrystals which can be doped with Mn ions as shown in schematic 1.2:

1. Conduction band of host nanocrystals lie well above the $^4\text{T}_1$ level.
2. Tune the band gap of host nanocrystals such that the conduction band crosses the $^4\text{T}_1$ level at some point with the increase in size (Band gap variation).

For the first case electronic structure is well established as Mn^{2+} *d-d* emission characteristic peak has been observed at ~ 2.12 eV with the long excitonic photoluminescence lifetime in milliseconds range. Here there is large energy difference between the dopant states and the band edge levels. These Mn doped colloidal nanocrystals are easy to synthesize and studying the emission mechanisms. The second case poses an interesting challenge in synthesis as well as in the study of emission mechanisms. Gamelin *et al.*^{23,38,39,42} have published several papers on Mn doped CdSe nanocrystals showing for the first time luminescence and lifetime studies at low temperature where the characteristic peak of Mn^{2+} is seen with the band edge peak at lower energy value. The photoluminescence of Mn doped CdSe nanocrystals have been studied as a function of the nanocrystals diameter. These nanocrystals have shown to be unique among



Schematic 1.2 shows the two cases possible when Mn^{2+} is a dopant ion.

colloidal doped semiconductor nanocrystals reported till date as in that quantum confinement allows in tuning of the CdSe band gap energy across the Mn^{2+} excited state energies. For smaller nanocrystals, the photoluminescence is mainly dominated by the Mn^{2+} emission while for larger nanocrystals; it has been dominated by CdSe excitonic emission. Magnetic circular dichroism (MCD) and magnetic circularly polarized luminescence (MCPL) spectroscopy independently confirms the existence of giant excitonic Zeeman splittings in these doped nanocrystals. Later report³⁸ on the same system came with the excitonic decay dynamics showing long excitonic photoluminescence decay times of up to 15 microseconds at temperature over 100 K. These decay times seems to exceed those of undoped CdSe quantum dots by approximately three orders

of magnitude which are supposed to be arising from the formation of excitons by back energy transfer from excited Mn^{2+} dopant ions. This observation though ignored in the original paper is strange because generally excitonic photoluminescence is quenched on the sub nanosecond time scale when the dopant states fall within the optical band gap of semiconductor. This suggests that Mn may indeed interact with the host. This is further corroborated by the observation of Viswanatha *et al.*⁴³ where direct correlation between the magnetic circular dichroism is found to surprisingly spin polarized the spin forbidden Mn^{2+} $d-d$ emission. This type of excitonic storage in the dopant state has not been observed before. This type of observation in which the excited state of dopant can interact with the conduction band of the semiconductor nanocrystals with thermal changes has not been seen in any other nanocrystals system. Figure 3, shows the model system proposed by Gamelin *et al.*³⁸ for their observations but still there is exactly no proof of this type interaction.

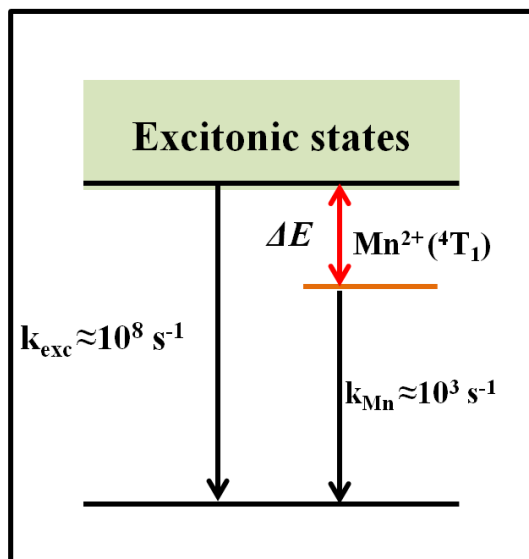


Figure 1.2. shows the proposed model system for Mn doped CdSe nanocrystals.

To completely understand these type of interactions taking place between the spin forbidden excited state of a dopant and conduction band of a semiconductor nanocrystals, a new type of host nanocrystals system needs to be chosen whose conduction band should be close enough to the 4T_1 state of manganese ion. Thus, alloyed Mn doped CdZnSe nanocrystals system has been chosen as the host nanocrystals to revisit this proposed model. In this work, we have systematically changed the band gap of the host nanocrystals by alloying Cd into ZnSe to study the mechanism of the Mn^{2+} Emission. This Cd alloying in the nanocrystals is done to bring the band edge levels close to the 4T_1 and 6A_1 state of the Mn^{2+} ion. The decay dynamics has been studied as a function of Cd incorporated in the Mn doped nanocrystals and it is evident that the host nanocrystals cannot be completely independent of Mn^{2+} emission as the band gap approached Mn^{2+} emission.

1.2.5 Co-doped Nanocrystal systems:

Co-doped nanocrystals are new class of nanomaterials which are expected to show unique and fascinating properties corresponding to the dopant ions been used. Co-doping in nanocrystals is relatively a new research area and not much has been explored. Co-doping means intentional introduction of two types of impurities in the nanocrystal lattice. This is a difficult phenomena as controlling the introduction, diffusion and interactions between the two different ions in a nanocrystals lattice poses a challenge in developing co-doped nanomaterials. There are not much literature reports on co-doping. Panda *et al.*⁴⁴ have shown co-doping of Mn and Cu in ZnSe nanocrystals which produces white light emission. Viswanatha *et al.*⁴⁵ have studied Fe/Cu co-doped ZnO nanocrystals which shows the double exchange between the Fe atoms which was mediated by the Cu atoms. Archer *et al.*⁴⁶ have observed strong sp-d exchange interactions in

colloidal Mn^{2+} and Co^{2+} doped CdSe quantum dots. Thus, each pair of transition metal dopants have showed different properties when co-doped in the host nanocrystals.

In this work, we have employed co-doping into a semiconductor with Manganese ions and another optically active dopant to study the mechanism in Mn and other transition metal emission. The other way in which the mechanism of Mn^{2+} ion emission can be studied is by introducing a second optically active ion like Cu, Ni, Co etc into the nanocrystals and study effect on the photoluminescence and decay dynamics of these co-doped nanocrystals to get a better understanding of the electronic structure responsible for specific type of emissions. For this, we have chosen the Ni^{2+} ions which give the broad emission peak centered around 650 nm and can be red shifted with the change in the band gap of the nanocrystals. Pradhan *et al.*² have shown successful incorporation of the Ni^{2+} dopant atoms in various semiconducting hosts with binary, alloyed and ternary composition. Thus, Ni^{2+} ions are versatile dopant that induces both optical as well as magnetic centers in various semiconducting host nanocrystals. Hence, Ni^{2+} ions have been used as a second optically active dopant.

The synthesis and characterization of Mn,Ni co-doped cadmium sulfide quantum dots (QDs) was done by Successive Ion layer Adsorption and Reaction (SILAR) method⁴⁷⁻⁴⁹. We have studied the optical properties and their photo dynamics by varying the concentration ratio of Mn: Ni in the nanocrystals system and this presence of another optically active ion i.e Ni in the system also helps in coming to the conclusion about electronic structure.

1.3 References and Notes

- (1) Karan, N. S.; Sarma, D. D.; Kadam, R. M.; Pradhan, N. *J. Phys. Chem. Lett.* **2010**, *1*, 2863-2866.
- (2) Jana, S.; Srivastava, B. B.; Jana, S.; Bose, R.; Pradhan, N. *J. Phys. Chem. Lett.* **2012**, *3*, 2535-2540.
- (3) Bhargava, R. N.; Gallagher, D.; Hong, X.; Nurmikko, A. *Phys. Rev. Lett.* **1994**, *72*, 416.
- (4) Nag, A.; Chakraborty, S.; Sarma, D. D. *J. Am. Chem. Soc.* **2008**, *130*, 10605-10611.
- (5) Hazarika, A.; Pandey, A.; Sarma, D. D. *J. Phys. Chem. Lett.* **2014**, *5*, 2208-2213.
- (6) Erwin, S. C.; Zu, L.; Haftel, M. I.; Efros, A. L.; Kennedy, T. A.; Norris, D. J. *Nature* **2005**, *436*, 91-94.
- (7) Norris, D. J.; Yao, N.; Charnock, F. T.; Kennedy, T. A. *Nano Lett.* **2001**, *1*, 3-7.
- (8) Pradhan, N.; Peng, X. *J. Am. Chem. Soc.* **2007**, *129*, 3339-3347.
- (9) Srivastava, B. B.; Jana, S.; Pradhan, N. *J. Am. Chem. Soc.* **2010**, *133*, 1007-1015.
- (10) Grandhi, G. K.; Tomar, R.; Viswanatha, R. *ACS Nano* **2012**, *6*, 9751-9763.
- (11) Pradhan, N.; Goorskey, D.; Thessing, J.; Peng, X. *J. Am. Chem. Soc.* **2005**, *127*, 17586-17587.
- (12) Raola, O. E.; Strouse, G. F. *Nano Lett.* **2002**, *2*, 1443-1447.
- (13) Qu, S. C.; Zhou, W. H.; Liu, F. Q.; Chen, N. F.; Wang, Z. G.; Pan, H. Y.; Yu, D. P. *Appl. Phys. Lett.* **2002**, *80*, 3605-3607.
- (14) Tiseanu, C.; Mehra, R. K.; Kho, R.; Kumke, M. *J. Phys. Chem. B* **2003**, *107*, 12153-12160.
- (15) Wolf, S. A.; Awschalom, D. D.; Buhrman, R. A.; Daughton, J. M.; Von Molnar, S.; Roukes, M. L.; Chtchelkanova, A. Y.; Treger, D. M. *Science* **2001**, *294*, 1488-1495.

- (16) Awschalom, D. D.; Kikkawa, J. M. *Physics Today* **1999**, *52*, 33-39.
- (17) Neal, J. R.; Behan, A. J.; Ibrahim, R. M.; Blythe, H. J.; Ziese, M.; Fox, A. M.; Gehring, G. A. *Phys. Rev. Lett.* **2006**, *96*, 197208.
- (18) Prinz, G. A. *Science* **1998**, *282*, 1660-1663.
- (19) Sun, Q.; Wang, Y. A.; Li, L. S.; Wang, D.; Zhu, T.; Xu, J.; Yang, C.; Li, Y. *Nat. Photonics* **2007**, *1*, 717-722.
- (20) Banin, U. *Nat. Photonics* **2008**, *2*, 209-210.
- (21) Gao, X.; Cui, Y.; Levenson, R. M.; Chung, L. W. K.; Nie, S. *Nat. Biotechnol.* **2004**, *22*, 969-976.
- (22) Chen, D.; Viswanatha, R.; Ong, G. L.; Xie, R.; Balasubramanian, M.; Peng, X. *J. Am. Chem. Soc.* **2009**, *131*, 9333-9339.
- (23) Beaulac, R.; Archer, P. I.; Ochsenein, S. T.; Gamelin, D. R. *Adv. Funct. Mater.* **2008**, *18*, 3873-3891.
- (24) Bol, A. A.; Meijerink, A. *Phys. Rev. B* **1998**, *58*, R15997.
- (25) Santra, P. K.; Kamat, P. V. *J. Am. Chem. Soc.* **2012**, *134*, 2508-2511.
- (26) Lin, J.; Zhang, Q.; Wang, L.; Liu, X.; Yan, W.; Wu, T.; Bu, X.; Feng, P. *J. Am. Chem. Soc.* **2014**, *136*, 4769-4779.
- (27) Nag, A.; Sapra, S.; Nagamani, C.; Sharma, A.; Pradhan, N.; Bhat, S. V.; Sarma, D. D. *Chem. Mater.* **2007**, *19*, 3252-3259.
- (28) Nag, A.; Sarma, D. D. *J. Phys. Chem. C* **2007**, *111*, 13641-13644.
- (29) Kim, J. H.; Holloway, P. H. *Adv. Mater.* **2005**, *17*, 91-96.
- (30) Schwartz, D. A.; Norberg, N. S.; Nguyen, Q. P.; Parker, J. M.; Gamelin, D. R. *J. Am. Chem. Soc.* **2003**, *125*, 13205-13218.

- (31) Viswanatha, R.; Sapra, S.; Sen Gupta, S.; Satpati, B.; Satyam, P. V.; Dev, B. N.; Sarma, D. D. *J. Phys. Chem. B* **2004**, *108*, 6303-6310.
- (32) Wang, Y. S.; Thomas, P. J.; O'Brien, P. *J. Phys. Chem. B* **2006**, *110*, 21412-21415.
- (33) Norberg, N. S.; Kittilstved, K. R.; Amonette, J. E.; Kukkadapu, R. K.; Schwartz, D. A.; Gamelin, D. R. *J. Am. Chem. Soc.* **2004**, *126*, 9387-9398.
- (34) Jin, Z.-W.; Yoo, Y. Z.; Sekiguchi, T.; Chikyow, T.; Ofuchi, H.; Fujioka, H.; Oshima, M.; Koinuma, H. *Appl. Phys. Lett.* **2003**, *83*, 39-41.
- (35) Mikulec, F. V.; Kuno, M.; Bennati, M.; Hall, D. A.; Griffin, R. G.; Bawendi, M. G. *J. Am. Chem. Soc.* **2000**, *122*, 2532-2540.
- (36) Sung, Y.-M.; Kwak, W.-C.; Kim, T. G. *Cryst. Grow. and Des.* **2008**, *8*, 1186-1190.
- (37) Kwak, W.C.; Sung, Y.-M.; Kim, T. G.; Chae, W.S. *Appl. Phys. Lett.* **2007**, *90*, 173111-173111-2.
- (38) Beaulac, R. m.; Archer, P. I.; Liu, X.; Lee, S.; Salley, G. M.; Dobrowolska, M.; Furdyna, J. K.; Gamelin, D. R. *Nano Lett.* **2008**, *8*, 1197-1201.
- (39) Beaulac, R. m.; Archer, P. I.; van Rijssel, J.; Meijerink, A.; Gamelin, D. R. *Nano Lett.* **2008**, *8*, 2949-2953.
- (40) Dalpian, G. M.; Chelikowsky, J. R. *Phys. Rev. Lett.* **2006**, *96*, 226802.
- (41) Du, M.-H.; Erwin, S. C.; Efros, A. L. *Nano Lett.* **2008**, *8*, 2878-2882.
- (42) Beaulac, R.; Archer, P. I.; Gamelin, D. R. *J. Solid State Chem.* **2008**, *181*, 1582-1589.
- (43) Viswanatha, R.; Pietryga, J. M.; Klimov, V. I.; Crooker, S. A. *Phys. Rev. Lett.* **2011**, *107*, 067402.
- (44) Panda, S. K.; Hickey, S. G.; Demir, H. V.; Eychmaller, A. *Angew. Chem.* **2011**, *123*, 4524-4528.

- (45) Viswanatha, R.; Naveh, D.; Chelikowsky, J. R.; Kronik, L.; Sarma, D. D. *J. Phys. Chem. Lett.* **2011**, *3*, 2009-2014.
- (46) Archer, P. I.; Santangelo, S. A.; Gamelin, D. R. *Nano lett.* **2007**, *7*, 1037-1043.
- (47) Sankapal, B. R.; Mane, R. S.; Lokhande, C. D. *Mater. Res. Bull.* **2000**, *35*, 177-184.
- (48) Reiss, P.; Protiere, M.; Li, L. *Small* **2009**, *5*, 154-168.
- (49) Yu, W. W.; Peng, X. *Angew. Chem. Int. Ed.* **2002**, *41*, 2368-2371.

Chapter 2

Study of Mn²⁺ *d-d* Emission mechanism in CdSe and CdZnSe host nanocrystals

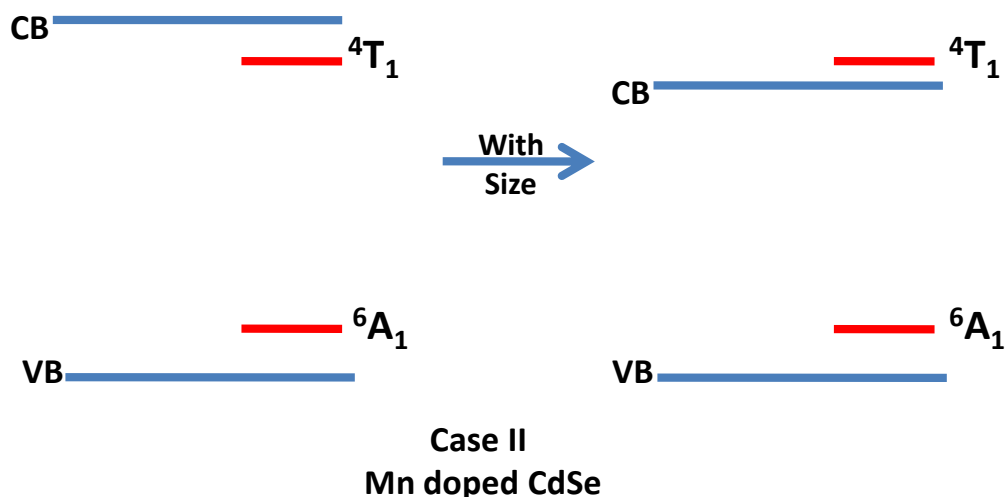
2.1 Abstract

Mn doped nanocrystals have now been studied for over a decade. Typically Mn doped systems show atomic like transition from 4T_1 level to 6A_1 in the photoluminescence spectra. This is a spin forbidden transition and it shows longer excitonic photoluminescence decay lifetimes of up to few hundreds of microseconds. This atomic transition is the intrinsic property of the Mn^{2+} ion and has been shown to be independent of the host nanocrystals in most cases. In this work, we have systematically changed the band gap of the host nanocrystals by alloying Cd into ZnSe to study the mechanism of the Mn^{2+} Emission. This Cd alloying in the nanocrystals is done to bring the band edge levels close to the 4T_1 and 6A_1 state of the Mn^{2+} ion. The decay dynamics has been studied as a function of Cd incorporated in the Mn doped nanocrystals and it is evident that the host nanocrystals cannot be completely independent of Mn^{2+} emission as the band gap approached Mn^{2+} emission. Temperature dependent luminescence studies have also been performed to get more insights of radiative and non-radiative relaxation processes occurring in these nanocrystals.

2.2 Introduction

Amongst the transition metal ion dopants, Mn^{2+} is the most studied dopant ion and has been doped in different types of host nanocrystals i.e. II-VI¹⁻¹², III-V^{9,13-15} and recently in multinary nanocrystals^{16,17}. Various nanocrystals like ZnSe, ZnS, CdS, ZnO, CdSe etc have hosted the Mn^{2+} impurity ions into their crystal lattice as observed from the signature emission peak at 2.12 eV arising from $Mn\ ^4T_1 \rightarrow ^6A_1$ transition. However, a similar observation has not been possible in CdSe nanocrystals with the exception of Gamelin's group¹⁸⁻²⁰. This has led to various theories trying to understand the reasons for being unable to dope Mn^{2+} in the CdSe crystal lattice.

Colloidal Mn^{2+} doped CdSe nanocrystals differ from all other colloidal doped semiconductor nanocrystals reported to date in that the band gap can be tuned across the Mn $d-d$ emission energy levels as a function of size. Gamelin *et al.*^{18,19} have shown that the energies of the Mn^{2+} ion and excitonic PL maxima as a function of nanocrystals diameter for a series of Mn^{2+} doped CdSe nanocrystals. They claimed that the energy of the excitonic transition depends strongly on particle size, but the energy of the localized Mn^{2+} transition does not. The characteristic $Mn^{2+}\ ^4T_1 \rightarrow ^6A_1$ emission is observed when the band gap energy is lower than the $d-d$ transition energy as evidenced in larger Mn doped CdSe nanocrystals. They also claimed that excitonic emission observed in the small Mn doped CdSe nanocrystals sample arises predominantly from undoped nanocrystals, which occur with greater probability as the nanocrystals diameter is reduced because of dopant exclusion from nuclei. Hence the nature of the emissive state changes at particular size marking the cross over from case I to case II (as discussed in chapter 1). These colloidal Mn^{2+} doped CdSe nanocrystals are unique in that they allow tuning from one type of case to the other quite readily, simply by changing the nanocrystal diameter. However, so far it is generally believed that due to the spin forbidden nature of Mn^{2+} emission, it doesn't interact with



Schematic 2.1 showing electronic structure variation for the Mn doped CdSe with nanocrystal size.

The host nanocrystals and there is no effect on the band edge emission as it approaches the Mn^{2+} $d-d$ transition energy. In this work, we wanted to verify this claim.

Hence we studied the mechanism of this Mn^{2+} emission using the host nanocrystals as CdSe and CdZnSe. This system is chosen as it can continuously vary the band edge levels of the host nanocrystals around the 4T_1 level of the Mn^{2+} ion. In this work, we have studied the Mn^{2+} emission mechanism with respect to the change in the host nanocrystals (CdZnSe) band gap by varying the Cd:Zn ratio and allowing different percentages of Cd to get incorporated inside the similar sized Mn doped CdZnSe nanocrystals. Excitonic decay dynamics have been studied for these nanocrystals to see the role of the atomic-type transition of Mn^{2+} ion and its interaction with the host with increasing Cd within the nanocrystals system. This is compared with undoped

CdZnSe nanocrystals of similar size where a gradual shift in the absorption and emission spectra starting from 410-550 nm is observed.

2.3 Experimental Section

2.3.1 Materials used:

Cadmium oxide CdO, zinc stearate $Zn(st)_2$, selenium shots, trioctyl phosphine (TOP, 90%), octadecene (ODE, 90%), oleylamine (Olam, technical grade 70%) were purchased from Sigma Aldrich. Stearic acid LR, manganous chloride AR ($MnCl_2$) were purchased from S D Fine chemicals limited. Tetramethyl ammonium hydroxide pentahydrate (TMAH, 98%) was purchased from Spectrochem. All purchased chemicals were used without further purification. Methanol, acetone and hexane were purchased from Merck (emparta). All solvents were used without further purification.

ZnSe Nanocrystals were prepared using zinc stearate as zinc precursor and TOPSe as the selenium precursor. For doping manganese, manganese stearate was used as a precursor. Cadmium stearate was used as a cadmium precursor.

2.3.2 Synthesis of Manganese stearate ($MnSt_2$):

$MnSt_2$ was synthesized as mentioned in literature⁵. Briefly, a conical flask was taken in which stearic acid (20 mmol) was dissolved in 20 g methanol by heating upto 50 °C and TMAH was dissolved in 20 g methanol in a separate flask. The acid solution was added to the TMAH solution and stirred for 20 min. Meanwhile, manganous chloride was dissolved separately in 10 g methanol and added dropwise to this mixture with constant stirring. The appearance of white precipitate shows the formation of $MnSt_2$. The solution was washed three times with methanol first and then four times with acetone by giving a gap of at least four hours in between. Then finally, white precipitate of $MnSt_2$ has been obtained.

2.3.3 Synthesis of Trioctyl Phosphine selenide:

Trioctyl phosphine selenide was synthesized as mentioned in literature⁵. All the processes were done inside the glove box. Selenium shots were weighed according to the concentration of the solution. These shots were then transferred to the vial containing a magnetic bar for stirring. 10 mL trioctyl phosphine solution was then poured into the vial. The vial was rubber capped and kept for stirring overnight. The solution was stirred till the all the shots dissolved completely. The resultant transparent solution is the Selenium precursor.

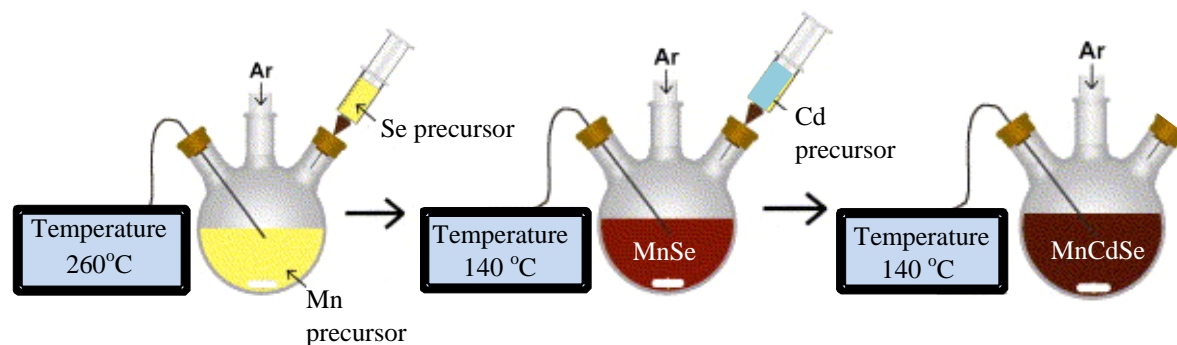
2.3.4 Synthesis of Cadmium stearate (CdSt₂):

CdSt₂ was synthesized using the similar synthesis method used for cadmium oleate⁵. Cadmium oxide was weighed and taken in the three necked round bottom flask with the calculated amount of stearic acid. ODE was added as a solvent (10 mL). The solution was then degassed for an hour at 100 °C and then filled with argon. The solution was heated till it became colourless at approximately to 260-280 °C. After this reaction was allowed to cool and the solution was collected in the argon filled vial at some moderate temperature (~100 °C). The solution solidified immediately after transferring to the vial. The solution was heated everytime before use.

2.3.5 Synthesis of Mn doped CdSe nanocrystals:

This synthesis was done with the nucleation doping method⁵. Here MnSt₂ was taken with ODE in the three necked flask. The reaction mixture was then degassed at 100°C for an hour. After purging with argon, the temperature was increased to 300°C followed by natural cooling till 140°C. As temperature reached 260°C, 0.5 mL of TOPSe (1.25 M) was added. When the temperature reached 140°C, 0.6 mL of CdSt₂ was added dropwise up to a minute. The reaction

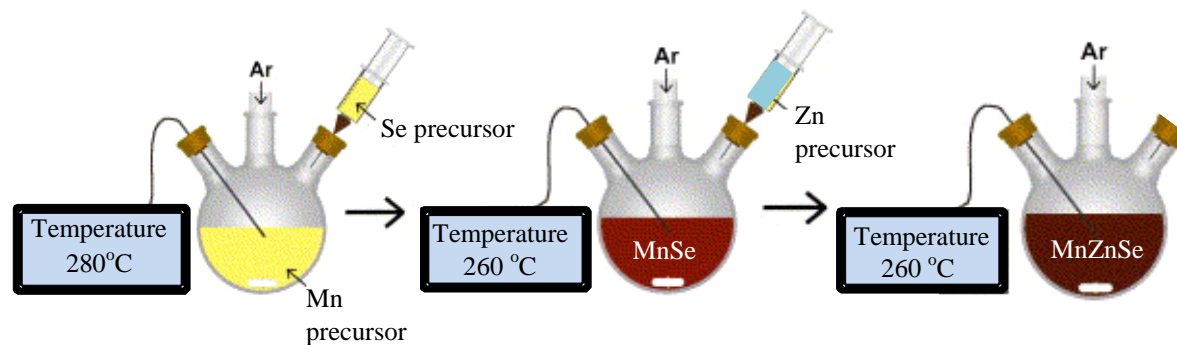
mixture was kept for nucleation and aliquots were collected at regular intervals to study the reaction. The sample was then washed with hexane and methanol thrice.



Schematic 2.2. Experimental setup of Synthesis of Mn doped CdSe nanocrystals.

2.3.6 Synthesis of Mn doped ZnSe nanocrystals:

Mn doped ZnSe nanocrystals were synthesized as mentioned in literature with the nucleation doping method⁵. Briefly, $MnSt_2$ (0.03 mmol) was taken in a three necked round bottom flask with the ODE as a solvent (10 mL). The solution was degassed for an hour at 100 °C and then filled with argon to increase the temperature. The temperature was increased to 280 °C and 0.5 mL TOPSe (1.25 mmol) was injected instantly into the round bottom flask and temperature was decreased to 260 °C. The reaction mixture was then kept for an hour. Meanwhile, $ZnSt_2$ (0.5 mmol) in ODE (1.2 mL) was taken in a separate vial and degassed and purged with argon. 0.6 mL of this $ZnSt_2$ solution was then added dropwise to the reaction mixture. The orange-red fluorescence in the UV light confirms the formation of the Mn doped ZnSe Nanocrystals. To increase the emission efficiency, 0.6 mL OlAm + ODE (1:1) solution was added to the mixture. The solution was dissolved in hexane and then washed with methanol twice.



Schematic 2.3. Experimental setup showing synthesis of Mn doped ZnSe nanocrystals.

Similar synthesis procedure has been followed with Mn doped CdSe nanocrystals.

2.3.7 Synthesis of Mn doped CdZnSe nanocrystals:

Mn doped ZnSe was synthesized as mentioned earlier. Following the addition of OIAm and ODE, the reaction mixture was maintained for 10 minutes at 260°C. The temperature was then decreased to 140 °C. Meanwhile, the different concentration solutions of CdSt₂ have been prepared using the stock solution in ODE. The cadmium precursor was then added using syringe pump for an hour and aliquots have been collected at different times.

2.3.8 Synthesis of Undoped CdZnSe nanocrystals:

Synthesis of undoped CdZnSe nanocrystals was similar to Mn doped counterparts. However instead of MnSt₂, same concentration of ZnSt₂ was used in the synthesis.

2.4 Characterization and Spectroscopic Studies

Nanocrystal structure and size identification of the particles was carried out using X-ray diffraction (XRD) and transmission electron microscopy (TEM).

TEM images were recorded using Technai F30 UHR version electron microscope, using a Field Emission Gun (FEG) at an accelerating voltage of 300 kV. Samples for TEM were prepared by adding a solution of the nanocrystals dissolved in toluene drop wise on carbon coated Cu grid. The solution was allowed to evaporate leaving behind the nanocrystals.

Crystal structure identification of the particles was carried out using X-ray diffraction, recorded on Bruker D8 Advance diffractometer using Cu K_α radiation. Since the diffracted intensities from these nanocrystals are generally weak, all patterns were recorded at a slow scan rate (0.75⁰ per minute) in order to get a high signal to noise ratio.

UV-Visible absorption spectra of various aliquots dissolved in hexane was obtained using Agilent 8453 UV-Visible spectrometer.

Steady state PL spectra were collected using the 450W Xenon lamp as the source on the FLSP920 spectrometer, Edinburgh Instruments while the lifetime measurements were carried out using microflash lamp and EPL-405 Picosecond Pulsed Diode Laser was used as excitation source ($\lambda_{\text{ex}} = 405 \text{ nm}$).

Low temperature measurements were done using optistat DN2, oxford instrument. Samples for low temperature measurements were prepared by drop casting a solution of the washed nanocrystals dissolved in hexane on glass slide. The solution was allowed to evaporate leaving

behind a film of nanocrystals on glass slide. Glass slide was cooled down to 80K and measurements were done at every 20K interval while increasing temperature to 300K.

Perkin Elmer Inductively coupled plasma-Optical emission spectroscopy (ICP-OES) has been used to obtain the elemental percentages present in the nanocrystals.

2.5 Results and Analysis:

Mn doping in II-VI nanocrystals has been extremely well studied in various host semiconductors. In all these systems, the successful doping of Mn²⁺ into the lattice of the semiconductor has been characterized by the presence of signature emission peak at 2.15 eV associated with the spin forbidden Mn *d-d* transition. Though, this peak was originally thought to be independent of host matrix and hence not tunable. It has recently been found that it can indeed be tuned^{21,22}. However, one system that has largely eluded this scrutiny is Mn doped CdSe nanocrystals. With the exception of one group^{18,19}, the signature Mn emission has not been observed by any group. Hence it has been assumed that Mn has not been incorporated into CdSe lattice. Here in this work, we have revisited this problem and compared with Mn doping in ZnSe nanocrystals. Mn doped CdSe and ZnSe nanocrystals were synthesized using the nucleation doping strategy. The formation of CdSe and ZnSe were characterized using X-ray diffraction.

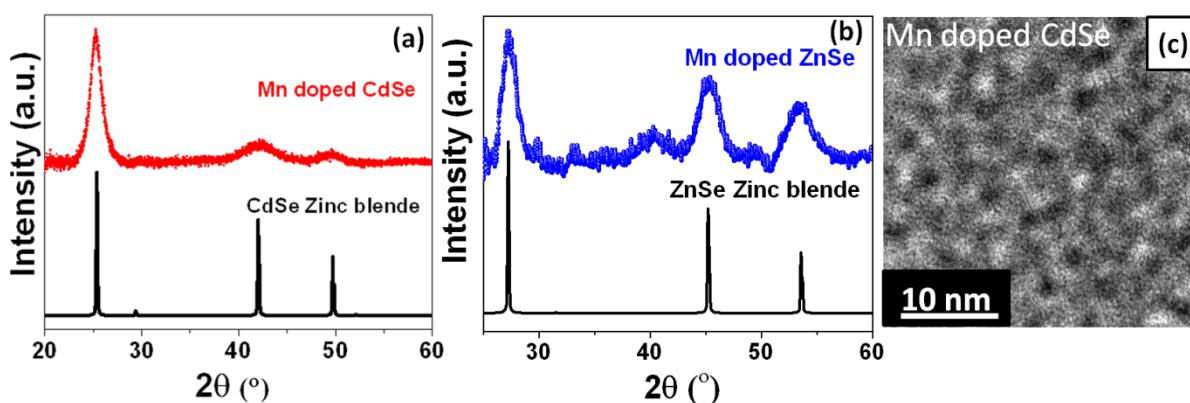


Figure 2.1. (a) shows XRD pattern of the Mn doped CdSe (red). (b) shows the XRD pattern of the Mn doped ZnSe nanocrystals. (c) shows TEM image of Mn doped CdSe nanocrystals shows average nanocrystals size to be 3.1 nm.

Figure 2.1 (a) and (b) shows the X-ray diffraction pattern of the Mn doped CdSe and ZnSe crystal structure nanocrystals as well as the bulk zinc blende crystal structure for both CdSe and ZnSe. The good agreement with the bulk structure proves the formation of zinc blende CdSe and ZnSe nanocrystals. The width of the peaks shows the signature of smaller size of the nanocrystals. Typical images of Mn doped CdSe nanocrystals are shown in figure 2.1 (c) which show that the average size of the nanocrystals to be around 3 nm. From the figure 2.1, it is evident that the required nanocrystals have formed.

Photoluminescence studies were performed on both the samples and are shown in figure 2.2. At room temperature, steady state emission of Mn doped ZnSe nanocrystals shows the characteristic Mn emission peak at 2.12 eV shown in figure 2.2 (a) while Mn doped CdSe nanocrystals doesn't show a clear peak similar to earlier reports^{2,23,24}. However it is also evident from the figure that Mn doped CdSe nanocrystals show asymmetry in the band edge peak which could be due to the

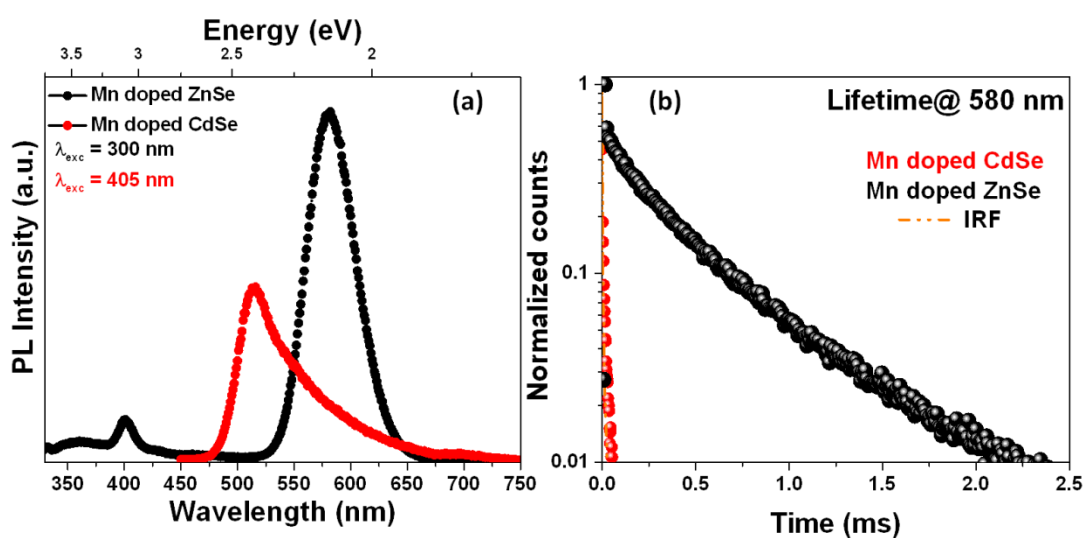


Figure 2.2.(a) shows room temperature photoluminescence studies of Mn doped CdSe (red) and ZnSe (black) with excitation wavelength as mentioned. (b) shows the lifetime studies of Mn doped CdSe and ZnSe nanocrystals taken emission at 580 nm.

contribution from Mn *d-d* transition. If that is indeed the case then it should show long lifetime at 580 nm. Figure 2.2 (b) shows the lifetime studies at 580 nm for Mn doped ZnSe and CdSe nanocrystals. The lifetime studies suggests that incorporation of the Mn²⁺ ions have taken place in the Mn doped ZnSe nanocrystals which shows the lifetime of ~0.4 ms corresponding to the spin forbidden transition (${}^4T_1 \rightarrow {}^6A_1$) while Mn doped CdSe shows no signature of long lifetime. This has been previously considered as a failure of Mn²⁺ to dope into CdSe

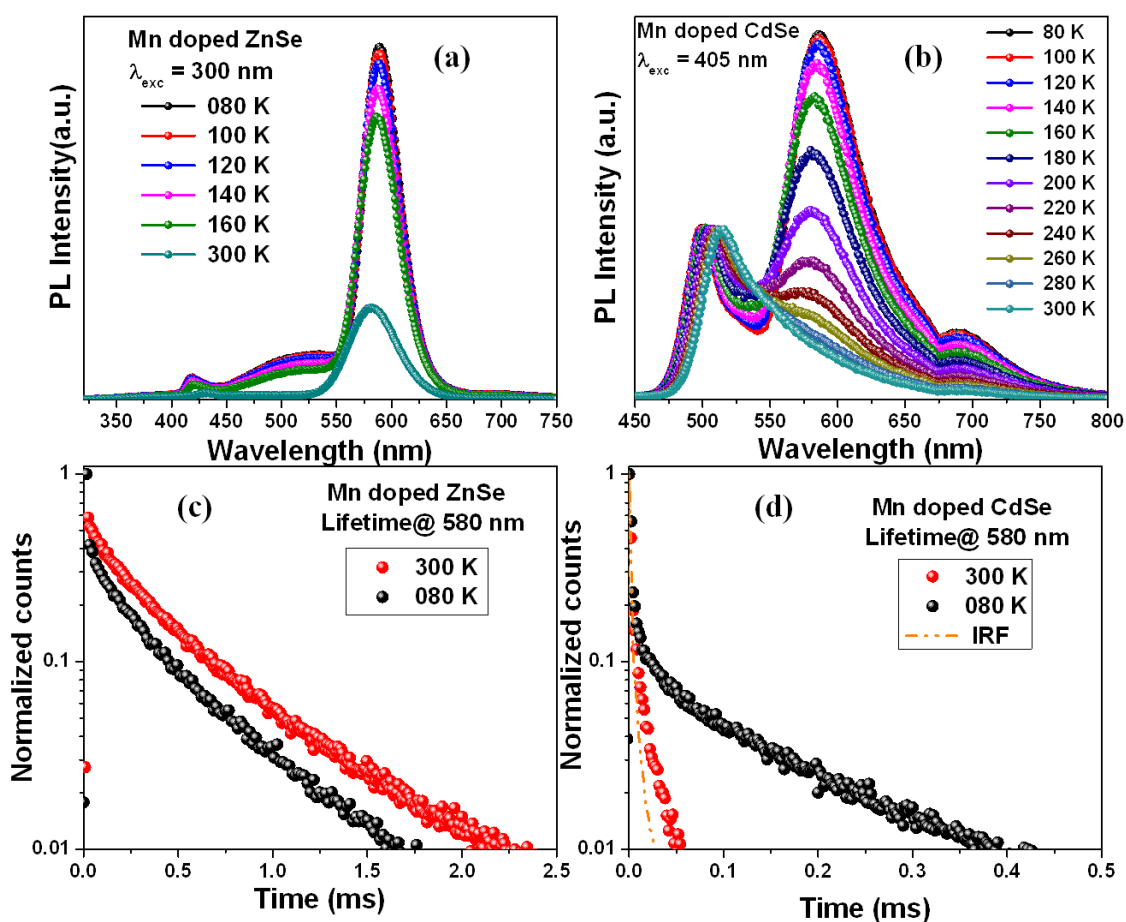


Figure 2.3. (a) and (b) shows the Temperature dependent photoluminescence studies of Mn doped CdSe and ZnSe nanocrystals respectively. (c) and (d) shows the Temperature dependent Time-resolved photoluminescence of Mn doped CdSe and ZnSe nanocrystals.

nanocrystals. But to understand the asymmetry in the band edge peak we performed the low temperature photoluminescence measurements. The same samples of both nanocrystals were then put for the low temperature photoluminescence measurements shown in figure 2.3. Figure 2.3 (a) and (b) shows the temperature dependent steady state emission and lifetime studies of Mn doped ZnSe nanocrystals. As expected, Mn doped ZnSe nanocrystals have shown the gradual increase in the intensity of the Mn emission as the temperature is decreased and a long lived lifetime of Mn *d-d* emission is essentially unchanged at 80 K as compared to the room temperature. Surprisingly, the low temperature data of Mn doped CdSe nanocrystals shown in figure 2.3 (c) and (d) shows the presence of a sharp emission peak at ~2.15 eV. In addition the lifetime shows a considerable increase amounting to ~150 microseconds at low temperature as seen from figure 2.3(c). This is surprising as this suggests that Mn is indeed present in CdSe nanocrystals and appears only at low temperature.

This, in fact, suggests the presence of a temperature mediated interaction with the host nanocrystals. Additionally, the proximity of band edge emission could play a key role in Mn²⁺ emission in 3D confined systems. Thus, in order to do a more systematic study of the same the band gap of the host nanocrystal has to be systematically tuned. The most obvious method is to make the nanocrystals smaller. However, these CdSe nanocrystals prepared here are quite small and it is non-trivial to make them even smaller in size. Therefore, we decided to systematically incorporate Cd into ZnSe crystal lattice and gradually shift them closer to the Mn²⁺ emission. The nanocrystals system chosen for the study was CdZnSe which shows the red shift or the decrease in band gap as more and more Cd gets incorporated in the ZnSe nanocrystals with no change in size of the nanocrystals.

Two sets of samples have been synthesized, namely undoped CdZnSe and Mn doped CdZnSe nanocrystals. Stoichiometrically calculated, different amounts of cadmium were added and the amount of cadmium got incorporated in the ZnSe crystal lattice was measured through ICP-OES

CdZnSe

	Stoichiometric Cd percentage	Measured Cd percentage (ICP)
Sample 1	2	0.1
Sample 2	5	0.5
Sample 3	40	2.0

Table 2.1. ICP-OES Data for Undoped CdZnSe nanocrystals

measurements. Table 2.1 shows the ICP-OES data of undoped CdZnSe nanocrystals which shows the amount of cadmium ion incorporated into the crystal lattice of ZnSe as compared to

MnCdZnSe

	Stoichiometric Cd percentage	Measured Cd percentage (ICP)
Sample 1	2	0.6
Sample 2	10	2
Sample 3	20	5
Sample 4	40	20

Table 2.2 ICP-OES Data for the Mn doped CdZnSe nanocrystals

the stoichiometric amount being added in the reaction mixture. Three samples of undoped CdZnSe nanocrystals with 0.1%, 0.5% and 2% Cd have been synthesized. Similarly, Table 2.2 shows the ICP-OES data of Mn doped CdZnSe nanocrystals. Here four samples of Mn doped CdZnSe nanocrystals with 0.6%, 2%, 5% and 20% Cd were synthesized.

These samples have been characterized using the X-ray Diffraction technique as shown in the fi-

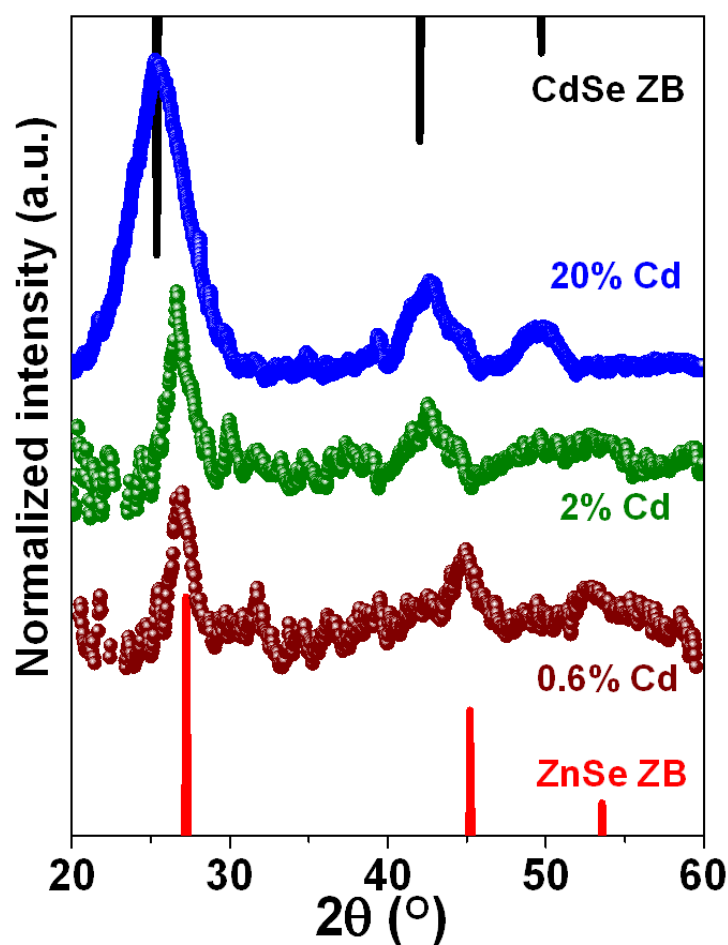


Figure 2.4. XRD pattern of the 0.6%, 2% and 20% Cd in Mn doped CdZnSe nanocrystals in comparison with ZnSe and CdSe zinc blende structure.

Figure 2.4 which shows the slow shifting of the XRD pattern from the ZnSe zinc blende structure to CdSe zinc blende structure with the increase in the Cd percentages from 0.6% to 20%. XRD pattern points towards the continuous alloying of the Cd ions inside the ZnSe crystal structure as peaks move towards the lower theta value becoming more like CdSe zinc blende structure. This shift in XRD is consistent with the ICP data which shows a similar increase in concentration of Cd. The broadness of the peaks shows the presence of the smaller sized nanocrystals which is consistent with the transmission electron microscopy (TEM). Figure 2.5 shows the TEM image

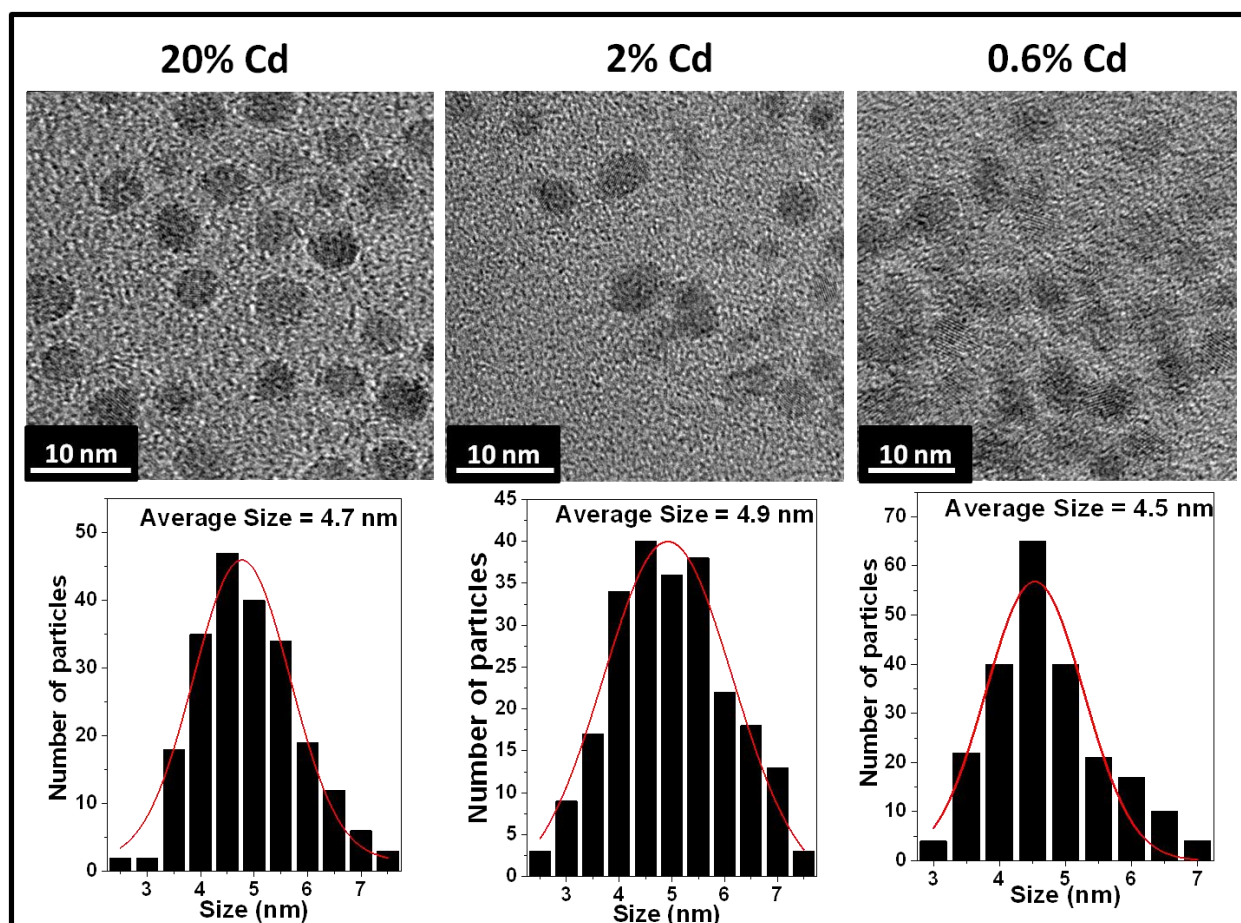


Figure 2.5 shows TEM images of 0.6%, 2% and 20% Cd in Mn doped CdZnSe nanocrystals with the average size of 4.5 nm, 4.9 nm and 4.7 nm respectively.

as well as the size analysis of the Mn doped CdZnSe nanocrystals for different percentages of Cd which prove that all the different Cd incorporated samples are of almost similar size. For the Size analysis, approximately 300 nanocrystals have been taken into consideration to get the average diameter of the nanocrystals. Histogram have been plotted and fitted with the Gaussian to calculate the average diameter for the different samples. Inductively coupled plasma optical emission spectrometer, X-ray diffraction and Transmission electron microscopy (TEM) shows the successful formation of the Mn doped CdZnSe and undoped CdZnSe nanocrystals of similar sizes. These samples are now used to study the optical properties.

Figure 2.6 shows the UV Visible and emission spectra of the undoped CdZnSe nanocrystals for different percentages of Cd. The undoped CdZnSe nanocrystals show the uniform shift towards the lower band gap. The emission shows that the peak started coming at 415 nm which was then

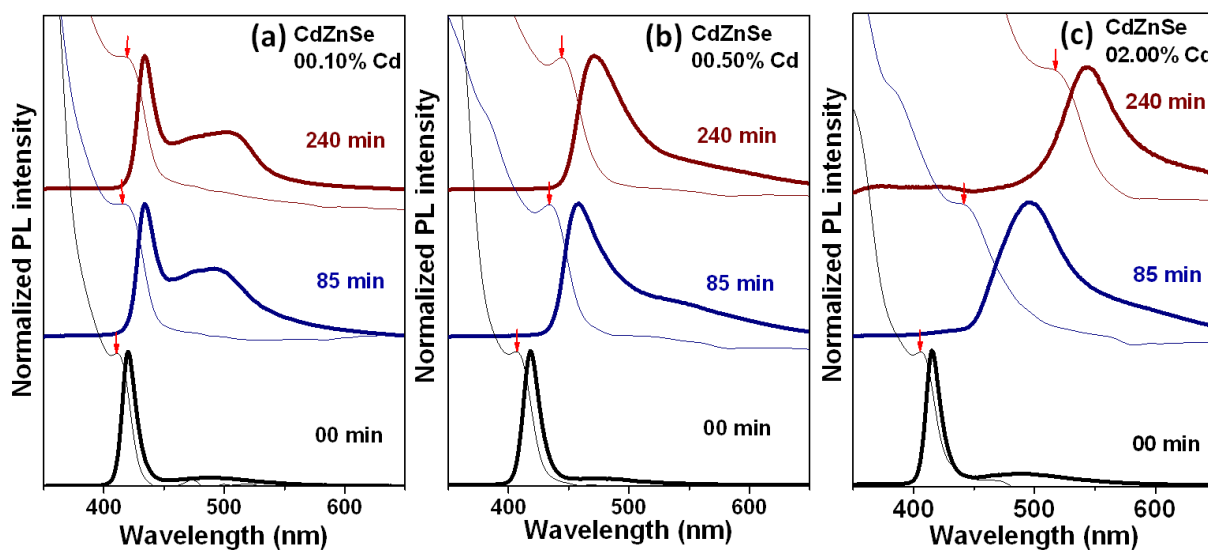


Figure 2.6. shows the UV visible absorption spectra and photoluminescence of three different Cd percent i.e. 0.1% Cd (a), 0.5% Cd (b), 2.0% Cd (c) alloyed CdZnSe.

can be tuned to 540 nm with just the 2 percent incorporation of Cd in the nanocrystals. The shift in the absorbance and emission spectra is in correspondence with the amount of incorporation of Cd in the nanocrystals. Similar synthesis of similar sized Mn doped CdZnSe shows a similar variation in absorbance spectra as shown by typical set of spectra in figure 2.7 (a). The increasing Cd incorporation as well as the evolution of band gap of Mn doped and undoped CdZnSe with reaction time is plotted as shown in figure 2.7 (b). The overlapping variation of band gap as a function of time suggests that the Mn doping does not alter the electronic structure of the host within this dilute limit as expected.

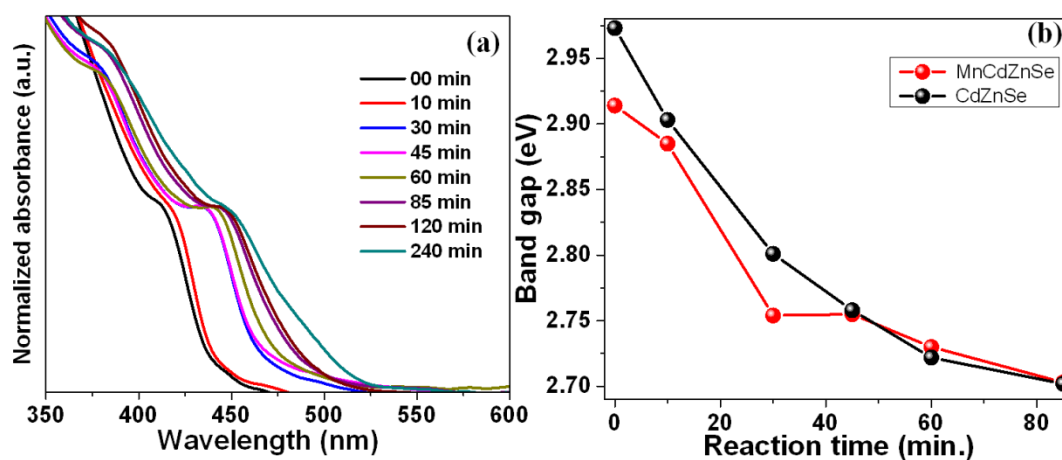


Figure 2.7. (a) shows UV Visible spectra of CdZnSe and MnCdZnSe which have almost similar sizes. (b) shows the red shift from 2.95 eV to 2.70 eV for CdZnSe and MnCdZnSe nanocrystals with time from 0 min. to 85 min.

The Mn doped CdZnSe nanocrystals were further studied at different time intervals by the photoluminescence spectra to study the evolution of Mn peak. Figure 2.8. shows the evolution of photoluminescence spectra for the case of 0.6%, 2% Cd, 5% and 20% Cd incorporation. It can be seen that an extra peak is raising in addition to the Mn^{2+} emission peak at about 500 nm. This

500 nm peak becomes more prominent than the Mn peak with increase in cadmium addition and reaction time.

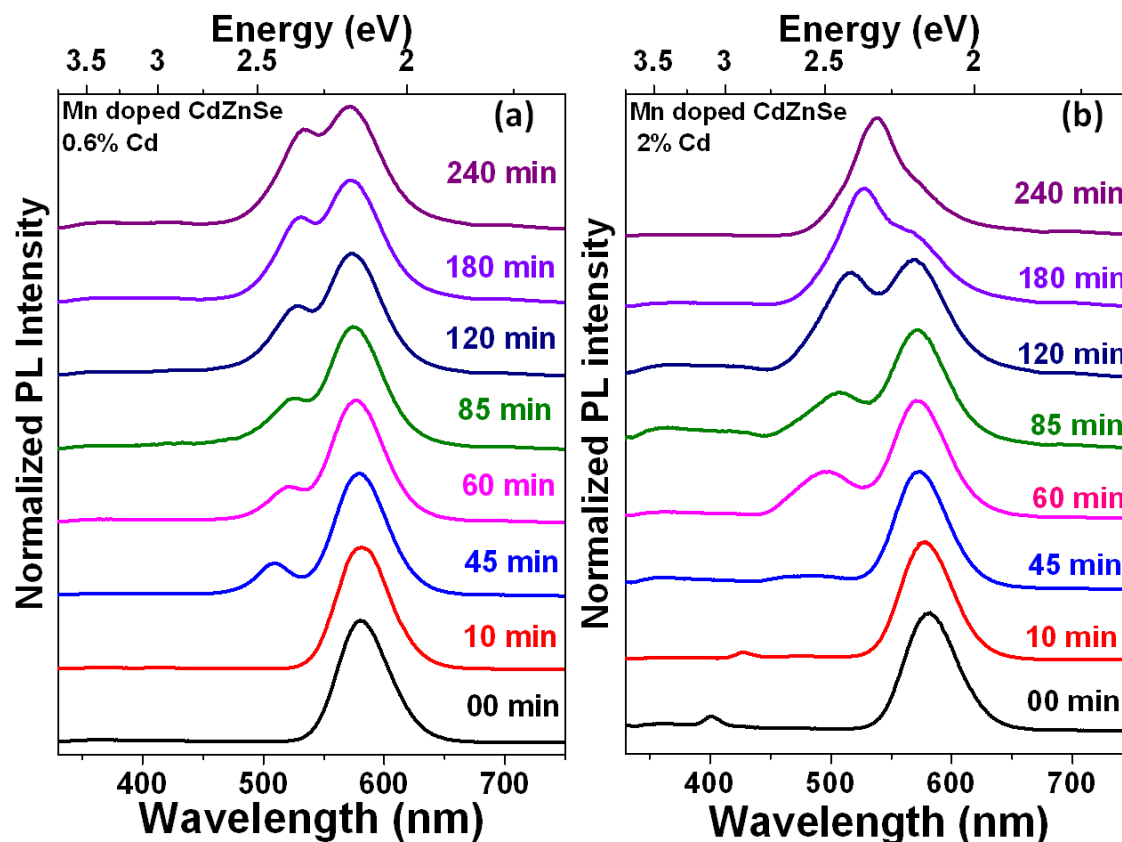


Figure 2.8.1 shows the evolution of the emission spectra for the (a) 0.6% and (b) 2% Cd in Mn doped CdZnSe nanocrystals with excitation wavelength of 300 nm.

With the increase in Cd percentages and time, this 500 nm peak red shifts towards the 580 nm peak eventually merging together into a single peak with a lifetime around a few nanoseconds. This growth rate of the 500 nm peak depends on the concentration of the cadmium precursor used. As seen from figure 2.8.2 (d), in the 20% Cd case, the two peaks becomes almost equal in intensity at 45 minutes while for 2% Cd precursor the peaks intensity becomes equal to each other at 120 minutes.

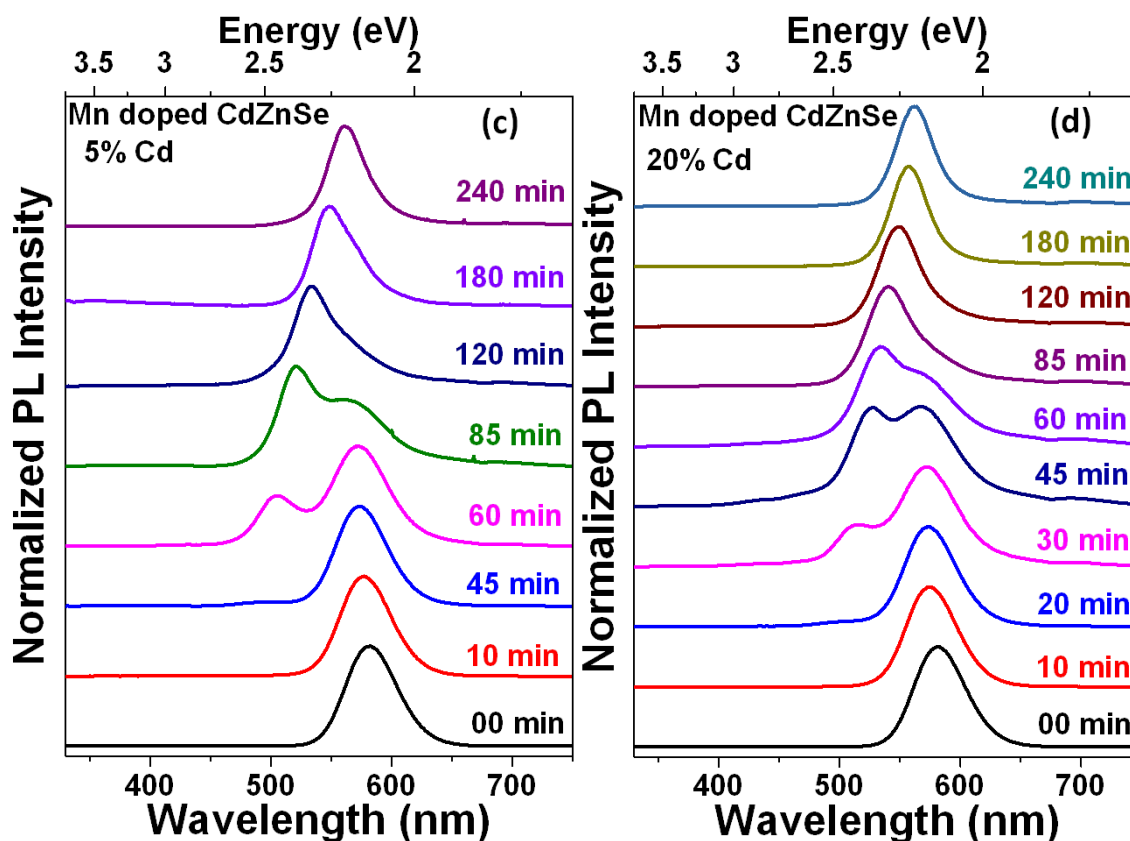


Figure 2.8.2 shows the evolution of the emission spectra for the (c) 5% and (d) 20% Cd in Mn doped CdZnSe nanocrystals with excitation wavelength of 300 nm.

Figure 2.9 shows the UV Visible and steady state emission spectra of 0.6%, 2% and 20% Cd with the lifetime at 580 nm for the 0 min. and 240 min. sample taken from micro flash lamp. The inset shows the lifetime of the 85 min. sample at 500 nm taken from the 405 nm Pulse diode laser. Surprisingly, unlike in the Mn doped CdZnSe, a peak always starts to rise at about 500 nm with lower intensity for lower concentration of Cd and higher intensity for greater cadmium percentages. This 500 nm peak has a lifetime in the order of nanoseconds shown in the inset of figures 2.8 (d), (e) and (f). and has been assumed to be band edge emission either from the doped or undoped fraction of the nanocrystals ensemble. This lifetime shows more features like a band

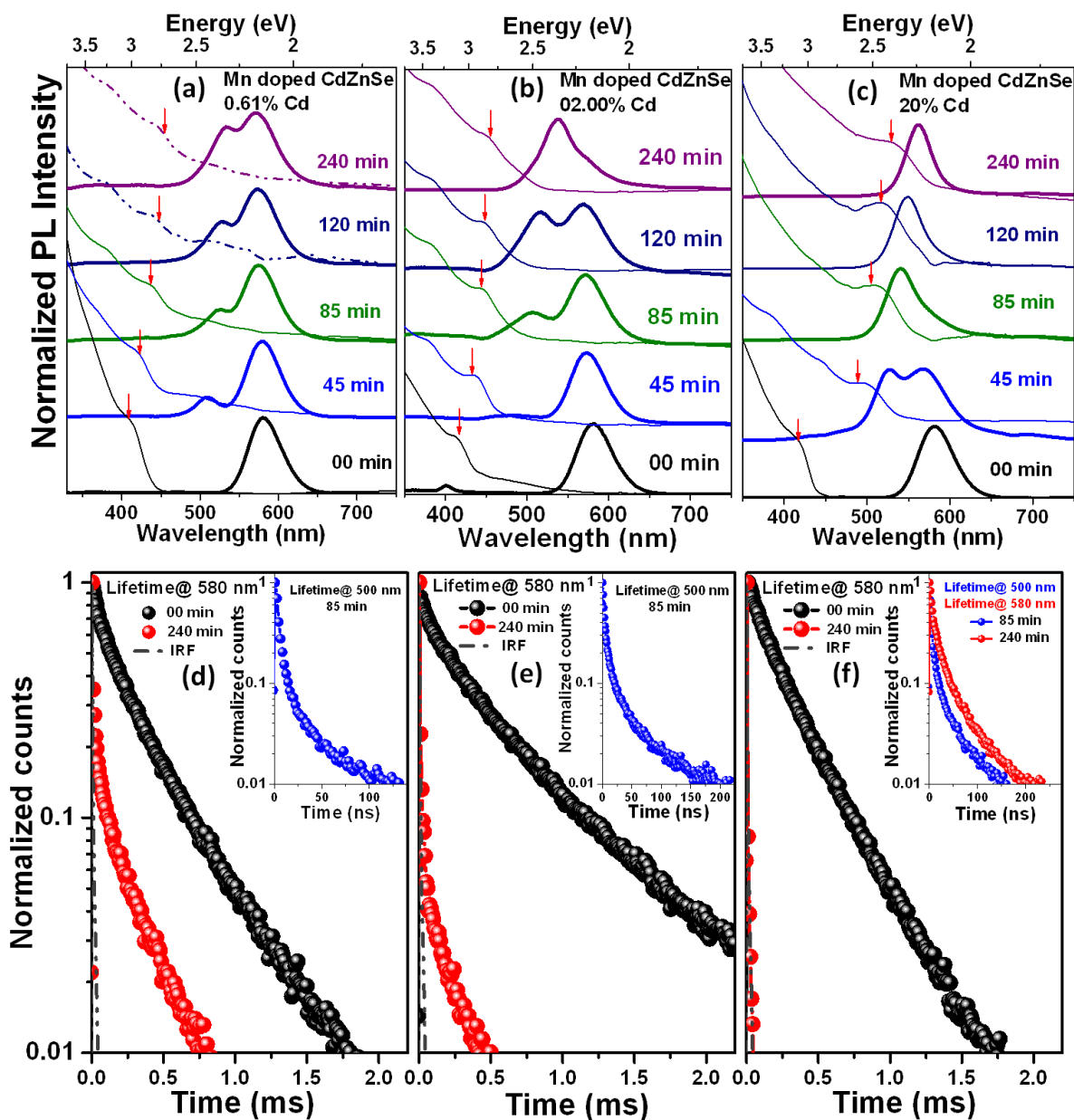


Figure 2.9. shows the UV Visible and emission spectra of the 0.61%, 2% and 20% Cd in Mn doped CdZnSe in the first row. Second row shows the corresponding lifetime at 580 nm for 00 min. and 240 min. (Inset: shows the lifetime at 500 nm for 85 min. sample)

edge but there seems to be little contribution of Mn²⁺ ions. Figure 2.9 also shows the lifetime studies taken at 580 nm for all the three cadmium alloyed percentages. In the synthesis, the cadmium precursor was added for an hour in all the cases starting with just Mn doped ZnSe

nanocrystals. The figure shows the lifetime studies of two typical samples i.e. 0 min. sample where there is no cadmium and 240 min. sample. At the time of Cd addition, Mn lifetime has been observed in all the three cases with microseconds lifetimes. However after 240 min. as the cadmium incorporation increases in the nanocrystals, the lifetimes also decreases and becomes more like IRF. In the case of larger percentages of Cd, in fact for 20% Cd as lifetime at 580 nm from microflash lamp looked like IRF was taken from laser as shown in the inset of figure 2.9 (f) which shows the band edge like features. This has so far assumed to be due to the diffusion of Mn^{2+} ions out of the lattice.

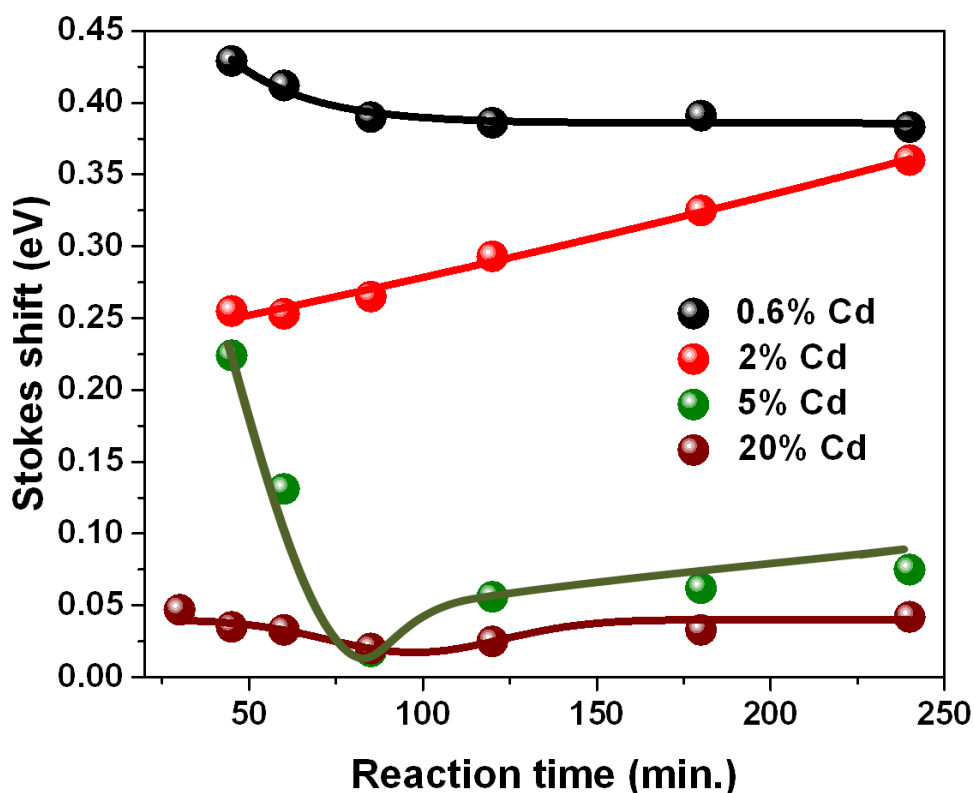


Figure 2.10. shows the change in the stokes shift calculated in eV for all the samples with reaction time (min.).

Figure 2.10. shows the change in the Stokes shift of the sample with respect to the reaction time consistent with the absorption and emission data, we observe that the Stokes shift decreases with the increase in the reaction time and then becomes constant while for the higher percentages of cadmium there seems to be an initial dip before which comes at different time for differently Cd alloyed sample and then a gradual increase in the Stokes shift. This is unlike that of undoped CdZnSe where the Stokes shift seems to be constant around 0.1 eV. Figure 2.12. (a) shows the increase in the area of 500 nm peak with respect to the normalized area of total peak for the passage of reaction. It has been observed from ICP that as the time proceeds, the area under the peak increases linearly and the slopes of this peak is linear with increase in Cd percentage as shown in figure 2.11 (b).

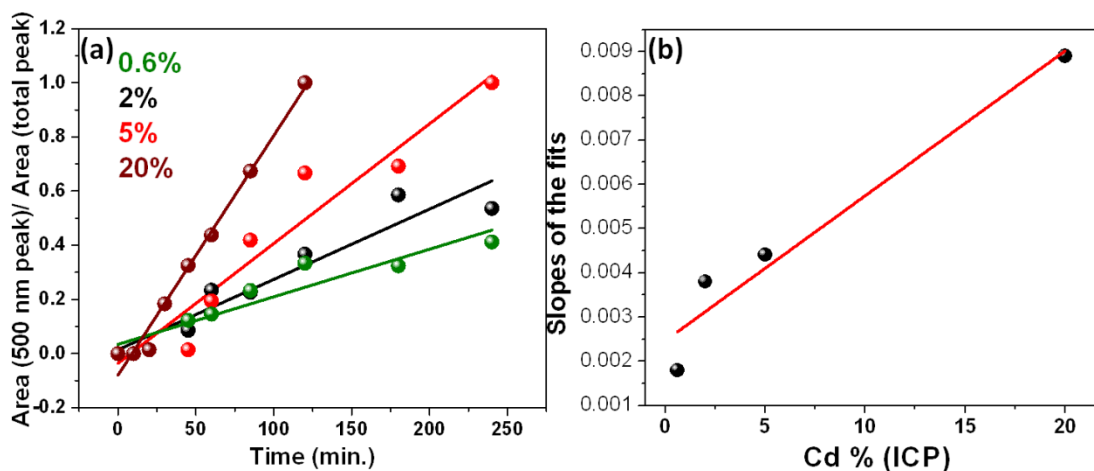


Figure 2.11. (a) Increase in the relative area of Cd peak with respect to reaction time for all samples. (b) Slopes of fitted line vs Cd% shows the evolution of Cd peak as Cd incorporation increases.

Thus, it can be said that slopes of the fits are directly proportional to the percentage of cadmium incorporation. This shows the clear linear dependence of slopes of the fits (relative area change

in Cd peak with respect to total area with reaction time) with the cadmium percentages as measured using ICP-OES.

Time-resolved photoluminescence measurements were taken to see how the lifetime varies in all the different percentages Cd incorporation in the Mn doped CdZnSe shown in figure 2.12. It is observed that the lifetime of Mn emission consistently decreases with increasing reaction time and percentage of cadmium eventually reaching the IRF. This suggests that the conduction band

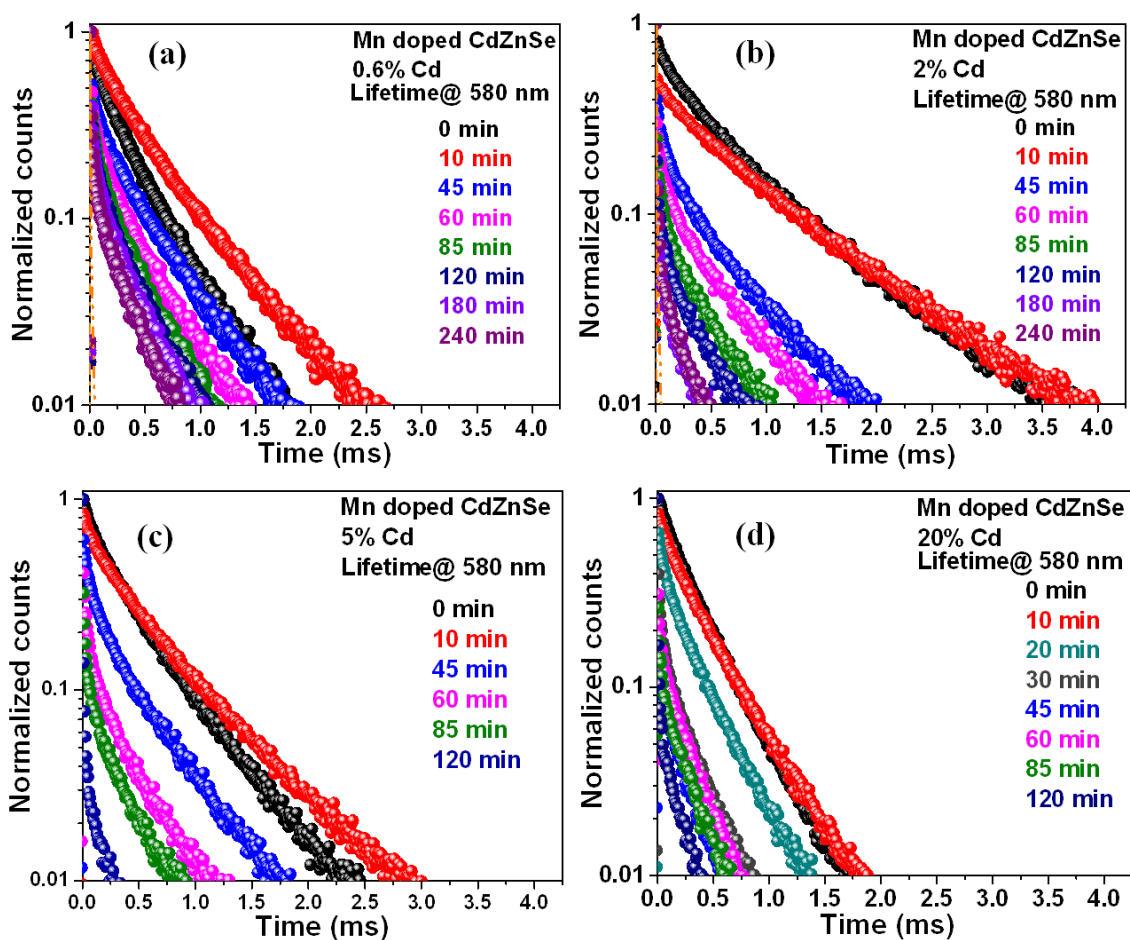


Figure 2.12. shows the change in the lifetime at 580 nm (Mn peak) for 0.6% Cd (a), 2% Cd (b), 5% Cd (c) and 20% Cd (d).

moves closer to the Mn *d-d* emission. There is a finite amount of band edge character in the Mn peak. For a more quantitative estimate, we have plotted the average lifetime as a function of time in figure 2.13.

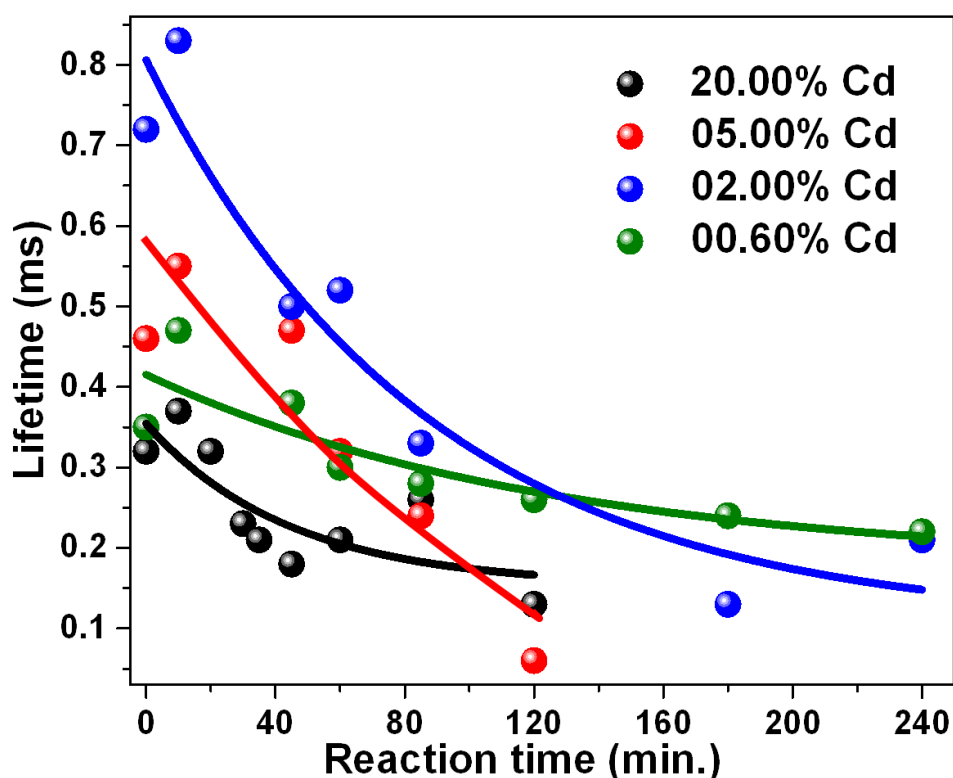


Figure 2.13. shows the lifetime variation of longer component (τ_1) with the reaction time for all Mn doped CdZnSe samples.

The lifetime decreases with the reaction time for all the samples. As more and more Cadmium gets incorporated inside the system the band gap of the host nanocrystals decreases, and the conduction band state of host nanocrystals interfering with the Mn *d-d* emission.

Effect of Size of Nanocrystals on Mn^{2+} emission- Different sizes of the Mn doped CdZnSe nanocrystals were synthesized to study how the Mn^{2+} emission changes as a function of size.

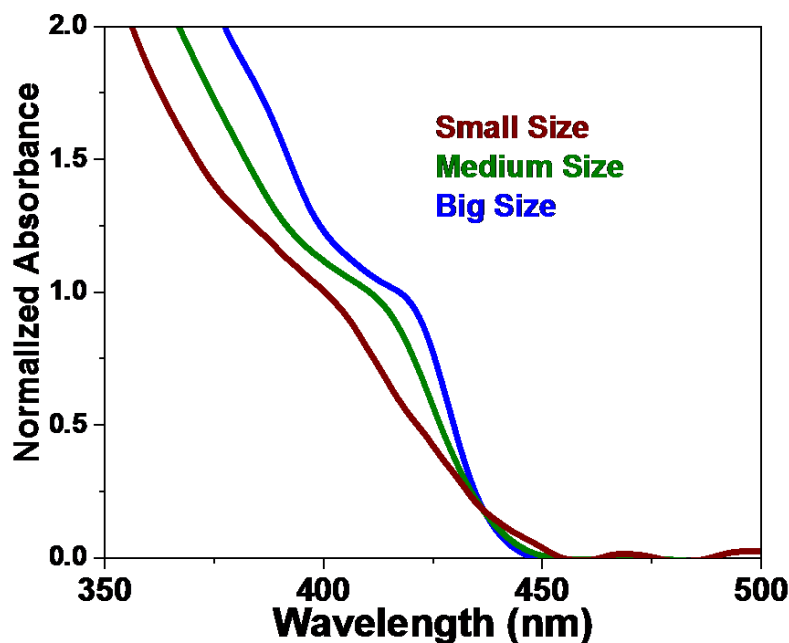


Figure 2.14. shows the UV Visible spectra of the different sized Mn doped CdZnSe nanocrystals.

Figure 2.14. shows the UV visible spectra of three different sizes of Mn doped CdZnSe nanocrystals. Growth of the nanocrystals was allowed at higher temperature; once a particular size is reached temperature has been decreased immediately to add the Cadmium precursor with different cadmium percentages. The size variation have been confirmed with the help of the UV Visible spectra which clearly shows the red shift as kept for longer time at higher temperature with the increase in size.

Figure 2.15. shows the photoluminescence spectra of all three different sizes of Mn doped CdZnSe nanocrystals with the same amount of cadmium incorporation i.e. 0.5% of Cd. Even

after incorporating equal amounts of cadmium in the nanocrystals, one can clearly make out the difference between the photoluminescence spectra of all the three cases. In the smaller size, the

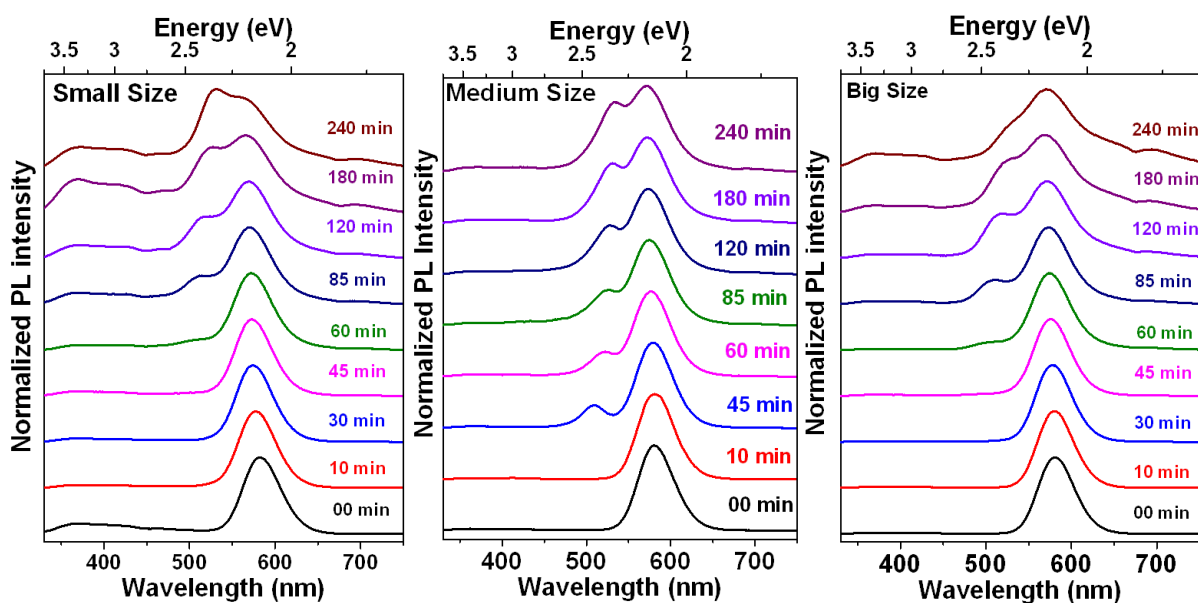


Figure 2.15. shows the Photoluminescence studies of different sized Mn doped CdZnSe nanocrystals.

peak rising at 500 nm became more intense than the Mn^{2+} emission peak in 240 minutes. Figure 2.17 (a) shows the shift in the higher energy peak in energy (eV) with respect to the reaction time (min.). The temporal evolution of the shift in the higher energy peak is almost same for all three different sizes which show that the shift is independent of the size of nanocrystals. On the other hand, when the temporal evolution of ratio under this peak to the total area was taken in figure 2.16 (b) which was observed to increase systematically with increasing size . Thus, this temporal evolution of ratio is dependent on the size of the nanocrystals. This shows the effect of size on the photoluminescence of the Mn doped CdZnSe nanocrystals.

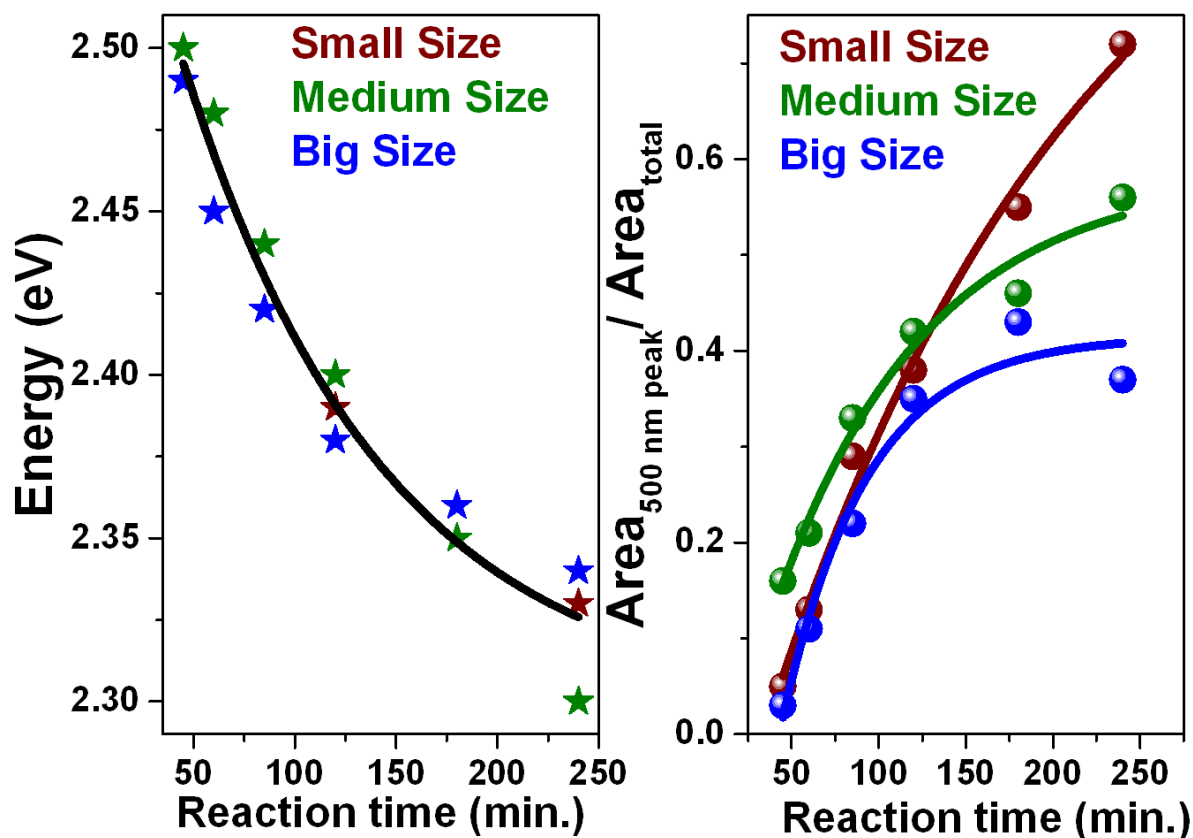


Figure 2.16. (a) shows the temporal evolution of 500 nm peak in energy (eV). (b) shows the temporal evolution of ratio Area of 500 nm peak to total area.

Low temperature Photoluminescence measurements- To study the role of temperature on the photoluminescence, two samples have been chosen from the 2% Cd in Mn doped CdZnSe nanocrystals i.e 2 hr sample in which the higher energy peak is far away from Mn peak and 4 hr sample in which it is closer to the Mn peak. Figure 2.18 (a) and (b) shows the low temperature photoluminescence measurements for the 2 hr and 4 hr sample from the 2% alloyed Cd in Mn doped CdZnSe respectively. The Photoluminescence intensity of the Mn peak increases as the temperature decreases which shows at the lower temperature there is lower degree of back

transfer from the spin forbidden 4T_1 state of the manganese ion to the first higher excited state. In the 2 hr sample, the Mn²⁺ emission was always more intense than the band edge peak at all temperatures suggesting that when band edge is far away from the Mn²⁺ emission, the excitons prefer to decay through the 4T_1 spin forbidden state which provides the longer lifetime. This also proves that there is no probability of back transfer of excitons in this case since there is a difference of sufficient amount of energy between the conduction band and 4T_1 dopant level. Thus, no interaction between the levels is possible in this case. In 4 hr sample, the conduction

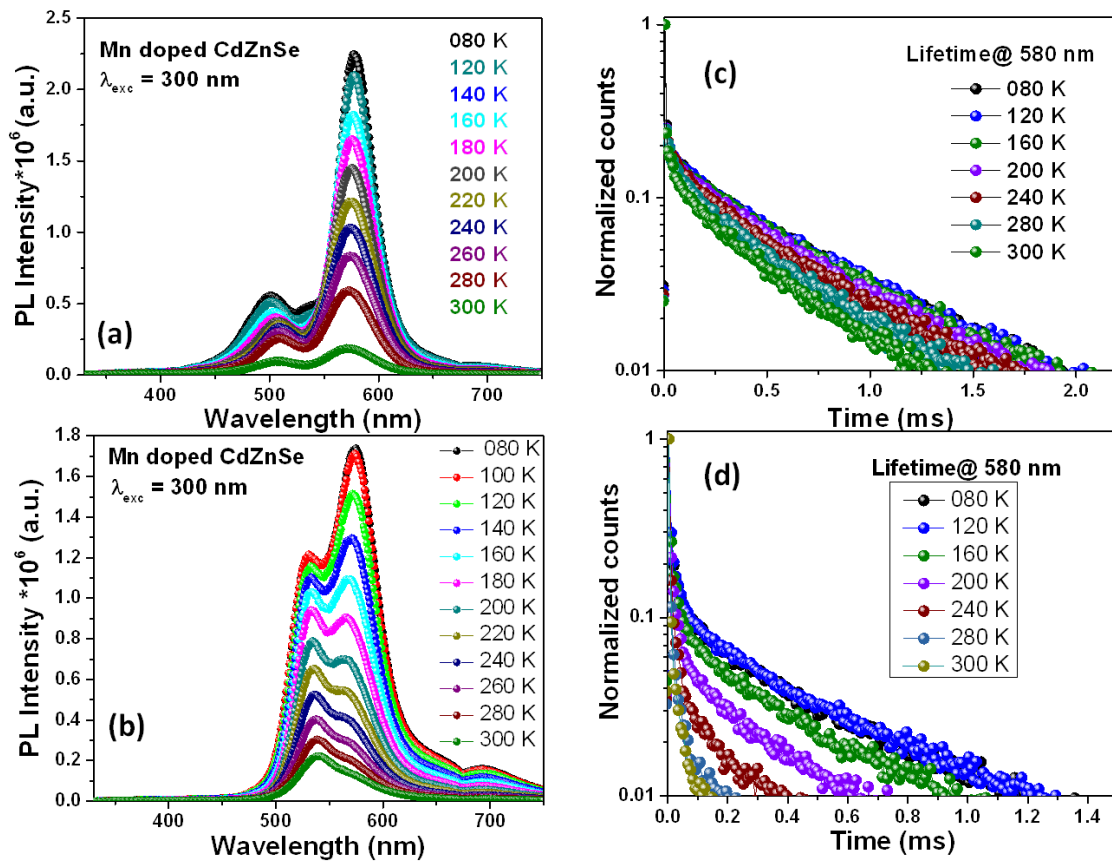


Figure 2.17. (a) and (c) shows the low temperature photoluminescence spectra for 2 hr and 4 hr sample respectively. (b) and (d) shows the lifetime studies of 2 hr and 4 hr sample respectively.

level is closer to the Mn^{2+} emission as shown in figure 2.17 (b). Here Mn^{2+} emission is intense than the band edge emission up to 160 K thereafter band edge emission becomes more intense for higher temperatures. Figure 2.17. (c) and (d) shows the temperature dependent lifetime measurements for the 2 hr and 4 hr samples respectively. The lifetime at 580 nm for 2 hr doesn't decrease much showing the decay through the Mn $d-d$ emission. Hence, when the band edge is far away from Mn^{2+} emission lifetime is independent of the temperature as also confirmed by figure 2.3 (d). But lifetime measurement for 4 hr shows the decrease in the lifetime as the temperature increases to 300 K. This decrease shows that the decay process which was dominating at lower temperature is not happening at the room temperature. Here it seems like at lower temperature decay was occurring through Mn $d-d$ transition and as temperature increases it

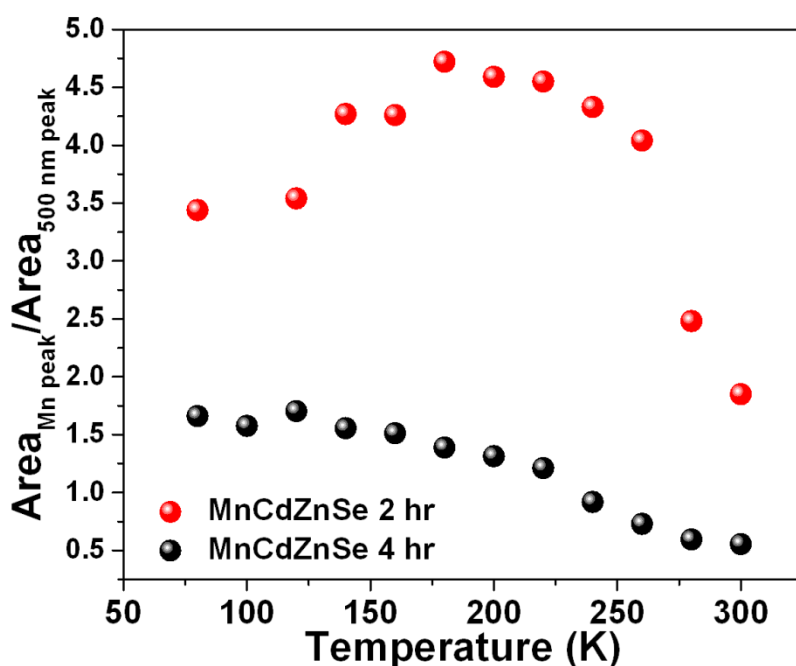


Figure 2.18. shows the variation in the area of Mn peak with respect to 500 nm peak over the series of temperatures.

appears that a back transfer is more facilitated from the Mn to the host. It should also be noted that the decay is longer than pure band edge decay. This shows that indeed there are some interactions taking place in this sample between the atomic excited state 4T_1 of Mn²⁺ ions and conduction band of host nanocrystals.

Figure 2.18. shows the variation of ratio of area under Mn peak to the area under band edge peak as a function of temperature. This graph shows that the ratio of areas of Mn peak to band edge peak follows the same trend for both 2 hr and 4 hr sample. As temperature increases from 80 K, ratio first increases then become constant till 260 K and then decrease once again. Comparably, there is larger difference in area in case of 2 hr sample than 4 hr sample as looks prominent from the temperature dependent photoluminescence spectra shown in figure 2.18. (a) and (c). Thus, low temperature photoluminescence measurements seem to have given more insight into the intrinsic mechanism occurring in these type of nanocrystals.

2.6 Discussions

Following the current data that we have on Mn^{2+} doped CdZnSe nanocrystals some points are evident. With the incorporation of cadmium, the photoluminescence peak rises at 500 nm and finally conquers the Mn peak showing clear variation in the band gap of host nanocrystals. However, though the lifetime studies shows the emergence of extremely fast component along with the longer component as well this peak doesn't energetically match directly to the band edge emission. Infact, it has been shown that this peak is actually insensitive to the variation of band gap. Temperature dependent measurements have shown that there is infact a temperature mediated back transfer of excited electrons between the spin forbidden Mn^{2+} level and the emission peak at 500 nm. Specifically, this internal transfer is strongest when the Mn *d-d* emission peak is in the proximity of the other peak. Keeping this in mind, it can be said that there can be two decay mechanisms that are possible:

1. Decay directly through spin forbidden Mn^{2+} level - The best method to see the actual emission the Mn is with the use of Gated photoluminescence measurements.
2. Decay through back transfer of excited electrons to the state giving rise to the 500 nm emission peak from spin forbidden Mn^{2+} level - This is probable as it explains the fast decay component. This has already been confirmed by low temperature measurements.

The main goal of this work is to study the Mn^{2+} *d-d* emission mechanism with respect to the host nanocrystals. In order to accomplish this a few more experiments with gated emission measurements are necessary.

2.7 Future work

After observing that there is indeed an interaction between Mn²⁺ atomic excited state with the conduction band of the nanocrystals, further studies will be focused on getting more insight into the decay dynamics mechanism involving *d-d* emission. We will do the gated photoluminescence measurements which will allow us to separate the two pathways taken by the excited electrons to decay to the ground state i.e. either electrons are getting de-excited through spin forbidden Mn²⁺ level or getting back transferred to the conduction band from the spin forbidden level and then getting de-excited. The increase of the fast component in the lifetime with Cd addition proves that the conduction band of the host nanocrystals is involved in some way. Gated photoluminescence measurements will allow us to see the decay after this fast component and hence may lead to interesting results.

Low temperature gated photoluminescence measurements will also be performed on some samples to see the effect of temperature on the decay dynamics of these nanocrystals. Thus, more studies need to be done to come to a final conclusion.

2.8 References and notes

- (1) Bhargava, R. N.; Gallagher, D.; Hong, X.; Nurmikko, A. *Phys. Rev. Lett.* **1994**, 72, 416.
- (2) Mikulec, F. V.; Kuno, M.; Bennati, M.; Hall, D. A.; Griffin, R. G.; Bawendi, M. G. *J. Am. Chem. Soc.* **2000**, 122, 2532-2540.
- (3) Norris, D. J.; Yao, N.; Charnock, F. T.; Kennedy, T. A. *Nano Lett.* **2001**, 1, 3-7.
- (4) Nag, A.; Sapra, S.; Nagamani, C.; Sharma, A.; Pradhan, N.; Bhat, S. V.; Sarma, D. D. *Chem. Mater.* **2007**, 19, 3252-3259.
- (5) Pradhan, N.; Peng, X. *J. Am. Chem. Soc.* **2007**, 129, 3339-3347.
- (6) Nag, A.; Chakraborty, S.; Sarma, D. D. *J. Am. Chem. Soc.* **2008**, 130, 10605-10611.
- (7) Acharya, S.; Sarma, D. D.; Jana, N. R.; Pradhan, N. *J. Phys. Chem. Lett.* **2009**, 1, 485-488.
- (8) Karan, N. S.; Sarma, D. D.; Kadam, R. M.; Pradhan, N. *J. Phys. Chem. Lett.*, 1, 2863-2866.
- (9) Radovanovic, P. V.; Barrelet, C. J.; Gradecak, S.; Qian, F.; Lieber, C. M. *Nano Lett.* **2005**, 5, 1407-1411.
- (10) Bussian, D. A.; Crooker, S. A.; Yin, M.; Brynda, M.; Efros, A. L.; Klimov, V. I. *Nat. Mater.* **2009**, 8, 35-40.
- (11) Pradhan, N.; Goorskey, D.; Thessing, J.; Peng, X. *J. Am. Chem. Soc.* **2005**, 127, 17586-17587.
- (12) Zeng, R.; Rutherford, M.; Xie, R.; Zou, B.; Peng, X. *Chem. Mater.* **2010**, 22, 2107-2113.
- (13) Somaskandan, K.; Tsoi, G. M.; Wenger, L. E.; Brock, S. L. *Chem. Mater.* **2005**, 17, 1190-1198.

- (14) Stowell, C. A.; Wiacek, R. J.; Saunders, A. E.; Korgel, B. A. *Nano Lett.* **2003**, *3*, 1441-1447.
- (15) Sahoo, Y.; Poddar, P.; Srikanth, H.; Lucey, D. W.; Prasad, P. N. *J. Phys. Chem. B* **2005**, *109*, 15221-15225.
- (16) Manna, G.; Jana, S.; Bose, R.; Pradhan, N. *J. Phys. Chem. Lett.*, *3*, 2528-2534.
- (17) Cao, S.; Li, C.; Wang, L.; Shang, M.; Wei, G.; Zheng, J.; Yang, W. *Scientific Reports* **2014**, *4*.
- (18) Beaulac, R. m.; Archer, P. I.; van Rijssel, J.; Meijerink, A.; Gamelin, D. R. *Nano Lett.* **2008**, *8*, 2949-2953.
- (19) Beaulac, R. m.; Archer, P. I.; Liu, X.; Lee, S.; Salley, G. M.; Dobrowolska, M.; Furdyna, J. K.; Gamelin, D. R. *Nano Lett.* **2008**, *8*, 1197-1201.
- (20) Beaulac, R.; Archer, P. I.; Ochsenein, S. T.; Gamelin, D. R. *Adv. Funct. Mater.* **2008**, *18*, 3873-3891.
- (21) Hazarika, A.; Pandey, A.; Sarma, D. D. *J. Phys. Chem. Lett.* **2014**, *5*, 2208-2213.
- (22) Hazarika, A.; Layek, A.; De, S.; Nag, A.; Debnath, S.; Mahadevan, P.; Chowdhury, A.; Sarma, D. D. *Phys. Rev. Lett.* **2013**, *110*, 267401.
- (23) Erwin, S. C.; Zu, L.; Haftel, M. I.; Efros, A. L.; Kennedy, T. A.; Norris, D. J. *Nature* **2005**, *436*, 91-94.
- (24) Norris, D. J.; Efros, A. L.; Erwin, S. C. *Science* **2008**, *319*, 1776-1779.

Chapter 3

Study of Mn^{2+} *d-d* emission mechanism in presence of other optically active ion (Ni^{2+})

3.1 Abstract

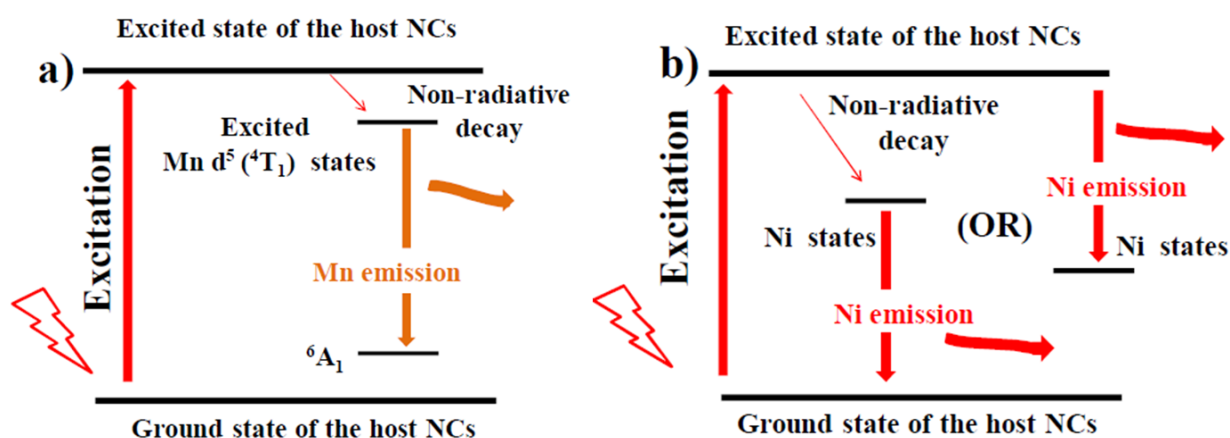
Recent advances in the synthetic chemistry opens up new ways of preparing doped nanocrystals with high quality which can be used for various potential applications. Co-doping of the nanocrystals is a challenging task but these co-doped nanocrystals can give rise to interesting optical, electronic and magnetic properties. Here we discuss the synthesis and characterization of Mn,Ni co-doped Cadmium Sulfide Quantum dots (QDs) by Successive Ion layer Adsorption and Reaction (SILAR) method. We studied their photo dynamics by varying the concentration ratio of Mn: Ni in the nanocrystals system. The presence of another optically active ion i.e Ni in Mn doped system can also be used to study the emission mechanism of Mn in semiconductor nanocrystals. The samples were characterized using ICP-OES, XRD and TEM. The optical properties were studied using UV-Visible absorption, steady state and time resolved photoluminescence. PL spectra of doped NCs differ from the undoped NCs with additional peak due to Mn²⁺ and Ni²⁺ ions without any detectable emission from the surface defects. Time resolved spectra shows high Mn lifetime in millisecond (ms) range in Mn doped QDs whereas Ni is having lifetime in microsecond (μ s) range in Ni doped QDs. Using this difference in lifetime we have studied the mechanism of Mn and Ni excitation and emission.

3.2 Introduction

Co-doping in the nanocrystals can give rise to very unique and interesting properties especially with the doping of transition metal ions in the nanocrystals¹⁻⁴. Manganese is the one of the most extensively studied transition metal dopant ion and have been doped in wide variety of host nanocrystals i.e. II-VI⁵⁻⁷, III-V^{8,9} and even in multinary nanocrystals¹⁰. The II-VI semiconductor nanocrystals doped with the Mn²⁺ ions shows an atomic like spin forbidden transition with the long excitonic photoluminescence lifetime in the range of milliseconds between the ${}^4T_1 \rightarrow {}^6A_1$ states. It has been observed that this atomic like transition remains unaffected with change in the host nanocrystals¹¹. Nickel has also been doped in the II-VI nanocrystals successfully¹². Ni²⁺ ions introduce a single dopant state in between the band gap of the host nanocrystals. This introduction of an extra impurity state in between the band gap changes the decay dynamics of the nanocrystals system.

The presence of more than one impurity states in the semiconductor nanocrystals generates the possibilities of multiple recombinations pathways and the actual pathway followed by the maximum number of excitons can be either selective, combined or the totally new pathway which can give different emission. The Mn levels lies in between the band gap of the II-VI semiconductor nanocrystals except in bulk CdSe where the band gap is smaller than the Mn *d-d* transition. But the position of the Ni²⁺ level is unknown relative to the band edge and Mn levels. Schematic 3.1 (a) shows the typical electronic structure of the Mn doped II-VI semiconductor nanocrystals where excitons gets transferred to the Mn levels with the non-radiative processes and decay with the longer lifetime to the ground state showing the characteristic Mn *d-d* emission. Ni doped nanocrystals shows the red shift of the dopant peak as the size of the nanocrystals increases with time. This tunability of the Ni dopant peak suggests that the Ni

impurities are providing a recombination pathway to the excitons which means there is an introduction of the new dopant state in between the band gap of the host nanocrystals. Schematic 3.1 (b) shows the two conditions that are possible for the position of Ni²⁺ ion state relative to the band edge. This state can be close to the conduction band or valence band depending upon the host nanocrystals. Pradhan *et al.*¹² have shown Ni²⁺ doping in different host nanocrystals having binary, alloyed and ternary composition. Following the tunability of the emission, that looks similar to the Cu doped systems^{13,14}. They have assumed Ni²⁺ is involved in the recombination process of the host exciton and on excitation the generated hole moves to close by impurity state and combines with the electron in the conduction band. Co-doping is also gives an alternative way to discover the relative electronic band structure of the nanocrystals system.



Schematic 3.1 (a) shows the typical electronic band structure of Mn doped II-VI semiconductor nanocrystals (b) shows the electronic structure of the Ni doped II-VI semiconductor nanocrystals.

In this work, to further study the mechanism of Mn *d-d* emission mechanisms, we have employed co-doping into a semiconductor with Mn and another optically active dopant Ni²⁺. Here we have chosen to co-dope Manganese and Nickel ions in the CdS nanocrystals using the

well established SILAR method¹⁵⁻¹⁷. These transition metal ions will provide more than one impurity states within the band gap of the CdS nanocrystals which will affect the decay dynamics of the excitons. This excitonic decay dynamics will show the contributions from both the optically active ions which have a difference in the lifetime of the order of some microseconds. Moreover, the relative position of the Ni²⁺ impurity level will be explored with respect to the Mn *d-d* levels and band edge levels of the host semiconductor nanocrystals.

3.3 Experimental Section

3.3.1 Materials used:

Cadmium oxide CdO, sulphur powder S, nickel acetate tetrahydrate $Ni (Ac)_2 \cdot 4H_2O$, octa decyl amine (ODA), octadecene (ODE, 90%) , oleic acid (Olac, technical grade 90%), trioctyl phosphine oxide (TOPO) were purchased from Sigma Aldrich. Stearic acid LR, manganous chloride AR ($MnCl_2$) were purchased from S D Fine chemicals limited. Tetramethyl ammonium hydroxide Pentahydrate (TMAH, 98%) was purchased from spectrochem. All purchased chemicals were used without further purification. Methanol, acetone and hexane were purchased from Merck (emparta). All solvents were used without further purification.

Cadmium sulphide was prepared using cadmium oleate and ODE in sulphur solution added after fixed interval of time. Manganese stearate and Nickel oleate are used as a dopant precursors.

3.3.2 Synthesis of Manganese stearate ($MnSt_2$):

$MnSt_2$ was synthesized as mentioned in literature¹¹. Briefly, a conical flask was taken in which stearic acid (20 mmol) was dissolved in 20 g methanol by heating upto 50 °C and TMAH was dissolved in 20 g methanol in a separate flask. The acid solution was added to the TMAH solution and stirred for 20 min. Meanwhile, manganous chloride was dissolved separately in 10 g methanol and added dropwise to this mixture with constant stirring. The appearance of white precipitate shows the formation of $MnSt_2$. The solution was washed three times with methanol first and then four times with acetone by giving a gap of at least four hours in between. Then finally, white precipitate of $MnSt_2$ has been obtained.

3.3.3 Synthesis of ODE-S:

0.2 M of sulphur solution has been prepared in 10 mL ODE. The solution is heated to $\sim 50^{\circ}C$ and sonicated to completely dissolve sulphur powder.

3.3.4 Synthesis of Nickel oleate ($NiOl_2$):

$NiOl_2$ has been synthesized using similar synthesis method used for Cadmium oleate as mentioned in literature reports¹⁸. Nickel acetate (0.408 g), Oleic acid (1.13 g) and ODE (7 mL) were taken in a cleaned three necked round bottom flask. The reaction mixture was kept for degassing at $80^{\circ}C$ for 90 minutes. After argon purging, the temperature was raised to $\sim 200^{\circ}C$ where colour change took place from colourless to green solution. This green solution of $NiOl_2$ was then transferred in a previously degassed vial. This $NiOl_2$ solution was used as a Ni precursor.

3.3.5 Synthesis of Cadmium oleate ($CdOl_2$):

$CdOl_2$ has been synthesized as mentioned in literature reports¹⁸. Cadmium oxide (0.320 g), Oleic acid (6.18 g) and ODE (9 mL) were taken in a cleaned three necked round bottom flask. The reaction mixture was kept for degassing at $80^{\circ}C$ for 90 minutes. After argon purging, the temperature was raised to $\sim 220^{\circ}C$ where colour change took place from brown to colourless solution. This colorless solution of $CdOl_2$ then transferred in a previously degassed vial. This $CdOl_2$ solution was used for overcoating shells.

3.3.6 Synthesis of Ni/ Mn doped CdS nanocrystals:

Ni doped and Mn doped CdS nanocrystals were synthesized using SILAR method as mentioned in literature^{15,17}. Nickel oleate (100 μ L)/ Manganese stearate (0.03 g) and ODE (8 mL) were taken in cleaned three necked round bottom flask. The reaction mixture was degassed at 80°C for 1 hr. 0.5 mL of 0.2 M ODE-S solution was mixed with 0.2 g of ODA and further diluted with 1 mL of ODE in a vial. After Ar purging, the temperature of reaction mixture was increased to 240°C. As temperature settles to 240°C, the precursor solution of S/ODA/ODE was injected quickly into the system. The temperature is then decreased to 140°C, for overcoating of the CdS layers. The Cadmium oleate (150 μ L) was added into the reaction mixture at a regular interval of 15 minutes. Minimum 12 layers have been grown on the core of NiS/MnS. Aliquots have been taken before the addition of Cd precursor each time. Samples were washed with 1:4 mixture of hexane: methanol and then re-dispersed in hexane for characterization.

3.3.7 Synthesis of Mn,Ni co-doped nanocrystals:

Mn,Ni co-doped nanocrystals were synthesized using SILAR method as mentioned in the literature^{15,17}. Manganese stearate, Nickel oleate (depending upon the Mn:Ni ratio) were taken together in a cleaned three necked round bottom flask with 12 mL ODE. This reaction mixture was kept for degassing at 80°C for 90 minutes. 0.5 mL of 0.2 M ODE-S solution was mixed with 0.2 g of ODA and further diluted with 1 mL of ODE in a vial. After Ar purging, the temperature of reaction mixture was increased to 240°C. As temperature settles to 240°C, the precursor solution of S/ODA/ODE was injected quickly into the system. The temperature is then decreased to 140°C, for overcoating of the CdS layers. The Cadmium oleate (150 μ L) was added into the reaction mixture at a regular interval of 15 minutes. Minimum 12 layers have been

grown on the core of NiS/MnS. Aliquots have been taken before the addition of Cd precursor each time. Samples were washed with 1:4 mixture of hexane: methanol and then re-dispersed in hexane for characterization.

3.4 Characterization and Spectroscopic Studies

Nanocrystal structure and size identification of the particles was carried out using X-ray diffraction and transmission electron microscopy.

TEM images were recorded using Technai F30 UHR version electron microscope, using a Field Emission Gun (FEG) at an accelerating voltage of 300 kV. Samples for TEM were prepared by adding a solution of the nanocrystals dissolved in toluene drop wise on carbon coated Cu grid. The solution was allowed to evaporate leaving behind the nanocrystals.

Crystal structure identification of the particles was carried out using x-ray diffraction, recorded on Bruker D8 Advance diffractometer using Cu K_α radiation. Since the diffracted intensities from these nanocrystals are generally weak, all patterns were recorded at a slow scan rate (0.75⁰ per minute) in order to get a high signal to noise ratio.

UV-Visible absorption spectra of various aliquots dissolved in hexane was obtained using Agilent 8453 UV-Visible spectrometer.

Steady state PL spectra were collected using the 450W Xenon lamp as the source on the FLSP920 spectrometer, Edinburgh Instruments while the lifetime measurements were carried out EPL-405 Picosecond Pulsed Diode Laser and microflash lamp was used as an excitation source ($\lambda_{\text{ex}} = 405 \text{ nm}$).

Low temperature measurements were done using optistat DN2, oxford instrument. Samples for low temperature measurements were prepared by drop casting a solution of the washed nanocrystals dissolved in hexane on glass slide. The solution was allowed to evaporate leaving

behind a film of nanocrystals on glass slide. Glass slide was cooled down to 80K and measurements were done at every 20K interval while increasing temperature to 300K.

Perkin Elmer Inductively coupled plasma-Optical emission spectroscopy (ICP-OES) has been used to obtain the elemental percentages present in the nanocrystals.

3.5 Results and discussions

For the synthesis of these doped nanocrystals, successive ion layer adsorption and reaction (SILAR) method has been used. Figure 3.1. shows the X-ray diffraction pattern of the Mn doped, Ni doped and Mn,Ni co-doped CdS nanocrystals as compared with bulk cubic structure of CdS. The broadness of the peaks suggests that the nanocrystals with finite size have been synthesized

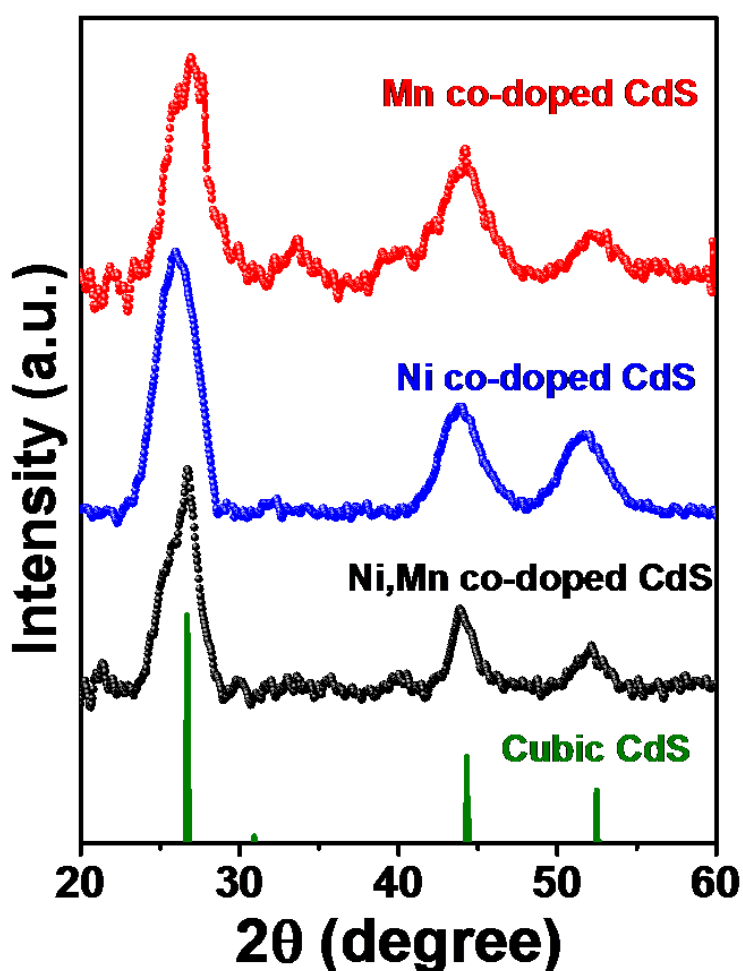


Figure 3.1. shows the X-ray diffraction pattern of the Mn doped CdS (red), Ni doped CdS (blue) and Mn,Ni doped CdS (black) compared with cubic CdS.

To further confirm the size of the nanocrystals Transmission electron microscopy (TEM) was performed. Figure 3.2. shows the TEM images for Mn doped CdS, Ni doped CdS and Mn,Ni co-doped CdS nanocrystals. The average diameter in case of Mn doped CdS, Ni doped CdS and Mn,Ni co-doped CdS was found to be 4.8 nm, 9.2 nm and 5.5 nm respectively.

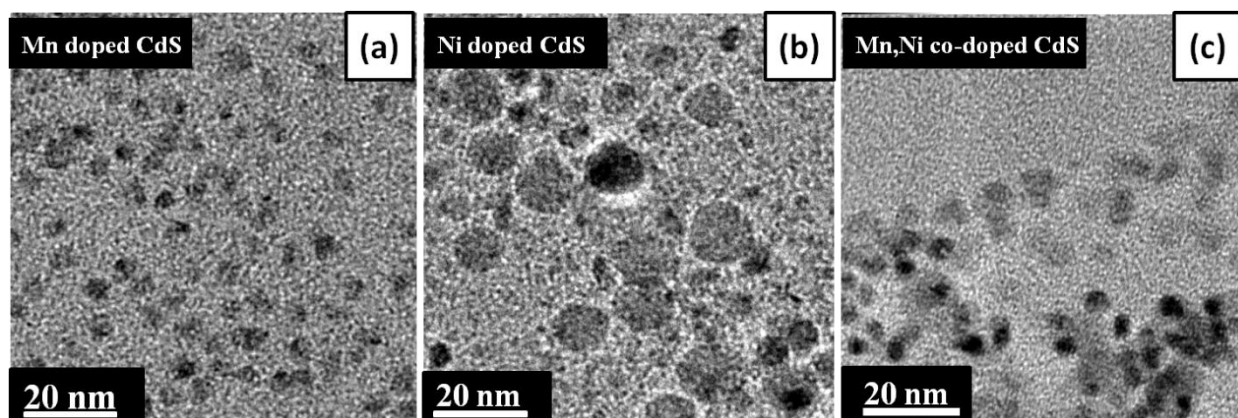


Figure 3.2. shows the TEM images of the (a) Mn doped CdS (b) Ni doped CdS (c) Mn,Ni co-doped CdS nanocrystals.

Figure 3.3. (a) shows the change in percentage of Ni and Cd as a function of number of shells of cadmium and sulphur added. Nickel seems to have leached out of the CdS nanocrystals with the increase in the number of shells and became 2% for 9th shell starting from the 18% in 1st shell. Figure 3.3. (b) shows the change in percentage of Mn and Cd as a function of number of shells. Manganese also seems to have leached out of the CdS nanocrystals with the increase in the number of shells and became 0.5% for 12th shell starting from the 96% in 1st shell. Both the transition metal ions used here have a tendency to diffuse out of the nanocrystal system as more

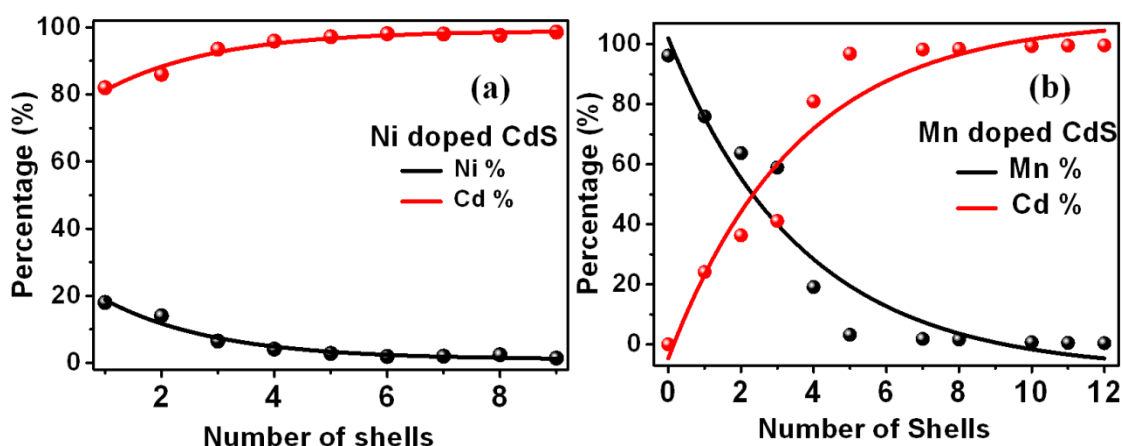


Figure 3.3. shows the ICP data for (a) Ni doped CdS (b) Mn doped CdS as a function of number of shells.

shells have been grown over. Figure 3.4 shows the variation in the ratio A/Cd percentage [$A = Mn, Ni$] with respect to the number of shells. The amount of manganese incorporated in the nanocrystals system is much more than the amount of Nickel that got incorporated inside the na-

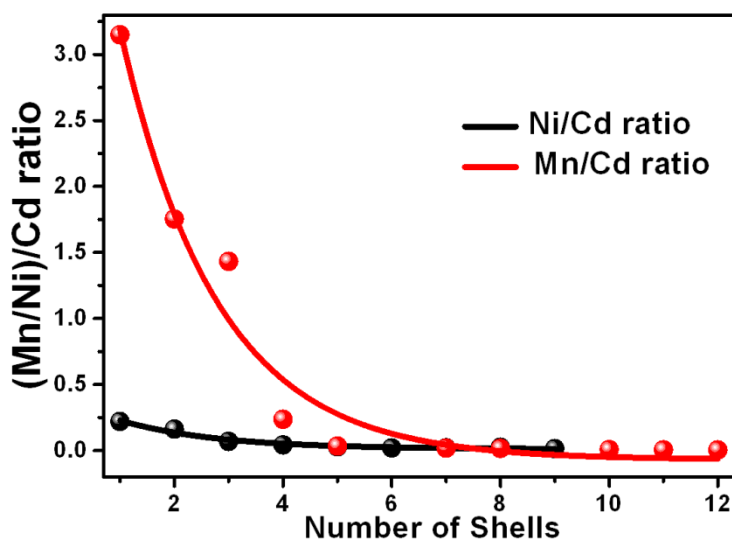


Figure 3.4. shows the variation of A/Cd ratio [$A = Mn, Ni$] as a function of number of shells.

-ocrystals. As the individual ions are showing the tendency to diffuse out of the system, it would be interesting to see how the rate of diffusion changes for both the ions when they are in the presence of each other confined in the nanocrystal regime. The same SILAR method has been used for the synthesis of Mn,Ni co-doped nanocrystals. The Stoichiometric ratio of the Mn: Ni was changed to study the change in the steady state emission spectra and decay dynamics variation with the help of the lifetime studies. ICP measurements were performed on the Mn, Ni co-doped system with different Mn: Ni ratio as shown in table 3.1 and it has been observed that both ions leach out of the nanocrystals system in presence of each other also. It is observed that Ni leach out faster and diffuse more than the Manganese ions.

	Stoichiometric percentages (Mn: Ni)	Measured percentages (ICP) (Mn: Ni)
Sample 1	98:2	90:10
Sample 2	90:10	76:24

Table 3.1. shows the comparison of ICP data with Stoichiometric amount for Mn,Ni co-doped Nanocrystals.

The X-ray diffraction pattern, TEM images and ICP shows the formation of the Mn doped CdS, Ni doped CdS and Mn,Ni doped CdS nanocrystals. To study the electronic structure of the these nanocrystals we have performed the steady state emission and lifetime measurements on these doped and co-doped samples.

As the shells were grown over the NiS core, the aliquots have been collected after addition of each shell into the reaction mixture. Before addition of the shells, there were no absorption and emission characteristics from the core as shells were increased the nanocrystals started to show

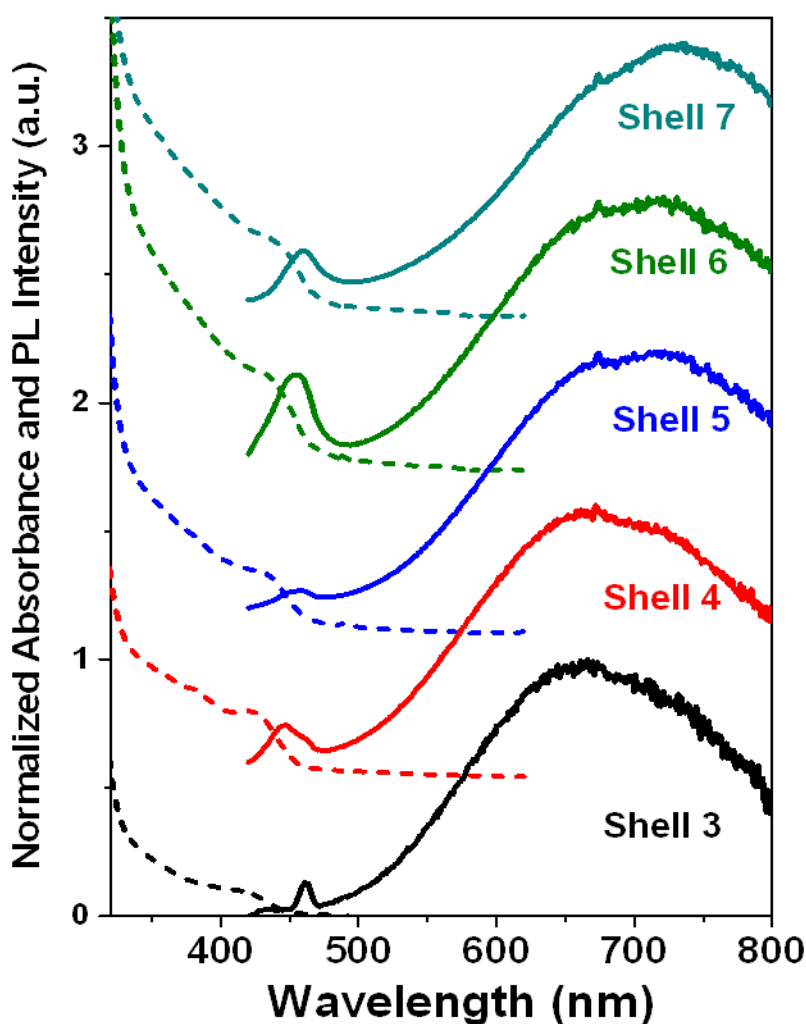


Figure 3.5. shows the UV visible and Steady state emission spectra for Ni doped CdS for various shells ($\lambda_{exc} = 405$ nm).

the emission characteristics of Ni^{2+} ion and CdS host nanocrystals. Figure 3.5. shows the absorption and emission from the Ni doped CdS nanocrystals. Absorption and emission features

have started coming up after the addition of the third shell. The band edge emission started coming at 460 nm and red shifted with the increase in the number of shells. A similar trend has been observed in the Ni^{2+} emission peak centred at 680 nm. This shift in the dopant peak tells that Ni has introduced a single state between the band gap of the semiconductor nanocrystals which can be closer to the conduction band or valence band which is not known at this point.

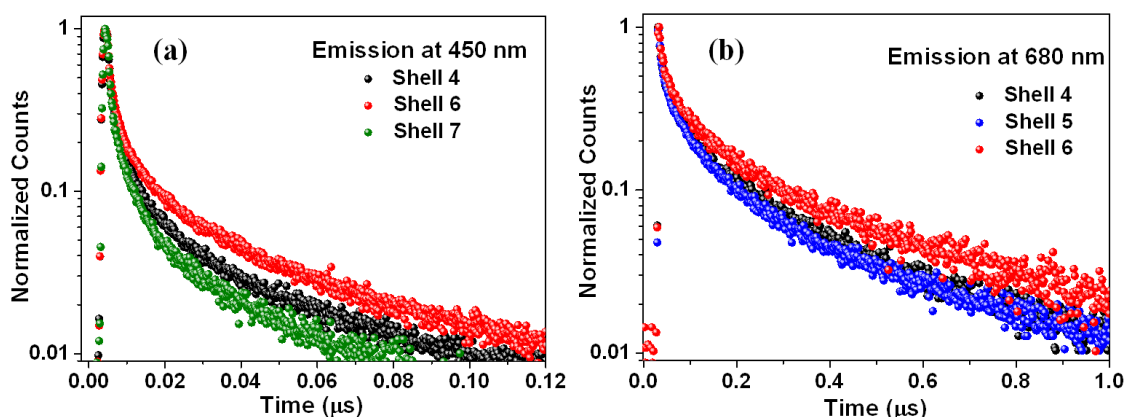


Figure 3.6. (a) shows the lifetime at 450 nm for Ni doped CdS (b) shows the lifetime at 680 nm for Ni doped CdS. $\lambda_{exc} = 405$ nm using pulsed diode laser.

Figure 3.6. (a) shows that the lifetime at 450 nm demonstrates a quick fall followed by a long lifetime component. This is not surprising as the Ni peak is quite broad and could still contribute to 450 nm. It is observed that the lifetime at the dopant peak at 680 nm does not change with the number of shells. The lifetime at the Ni^{2+} emission peak was found out to be in some hundreds of nanoseconds. The results show the successful incorporation of nickel ions in the CdS nanocrystals as characterized by the ICP measurements.

Figure 3.7. (a) shows the steady state emission spectra of the Mn doped CdS nanocrystals. The emission spectra shows the evolution of the band edge peak starting from 440 nm and shifting

towards higher wavelength with the increase in the number of shells. The other peak centred at 570 nm corresponds to the characteristic ${}^4T_1 \rightarrow {}^6A_1$ atomic like spin forbidden transition which doesn't change position with the change in the band gap of the host nanocrystals. This proves that this transition is happening between the two states introduced by the Mn²⁺ dopant ions which is the intrinsic property of that particular ion. Figure 3.7 (b) shows the lifetime taken at 570 nm for the Mn doped CdS nanocrystals. As expected the lifetime lies in the range of few tens of microseconds which is corresponding to the spin forbidden transition of the Mn²⁺ ions.

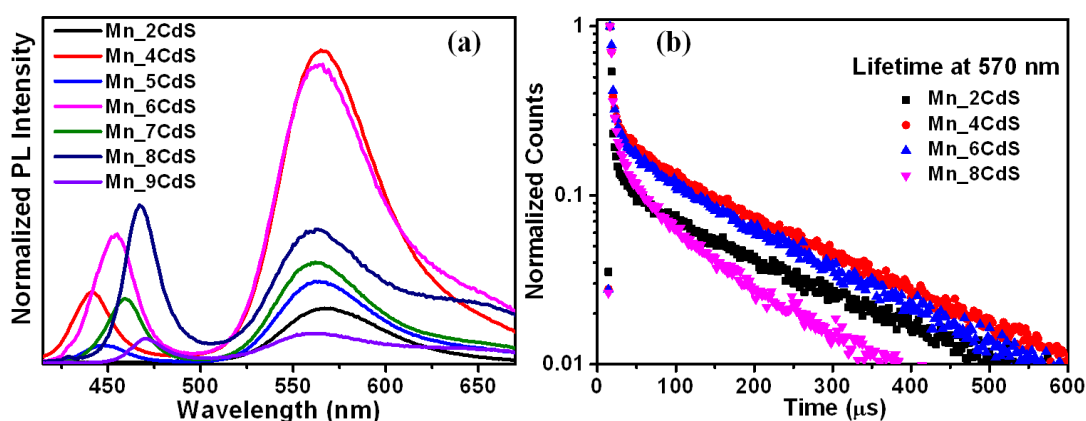


Figure 3.7. (a) shows the steady state emission spectra of Mn doped CdS nanocrystals ($\lambda_{exc} = 405$ nm) (b) shows the lifetime at 570 nm taken using 405 nm pulsed diode laser.

The steady state emission and lifetime measurements confirms the formation of Mn doped CdS nanocrystals. Thus, Ni doped and Mn doped CdS nanocrystals have been successfully synthesized and characterized using the ICP data, steady state emission spectra and time resolved photoluminescence measurements.

Figure 3.8 shows the steady state emission spectra for all the different Mn: Ni ratios synthesized stoichiometrically. The steady state emission for the Mn: Ni:: 98: 2 shows the intense manganese

characteristic peak at 570 nm with the emission peak of Nickel at 725 nm. This shows that excitons are decaying through both the channels available in the co-doped nanocrystals. Mn^{2+} emission is prominent when the Mn: Ni ratio is greater and as the ratio decreases, we see the intense nickel emission which shows that the more excitons are getting transferred to the Ni^{2+} state as shown in figure 3.8. (b). Even for lower Mn: Ni ratios, ICP-OES

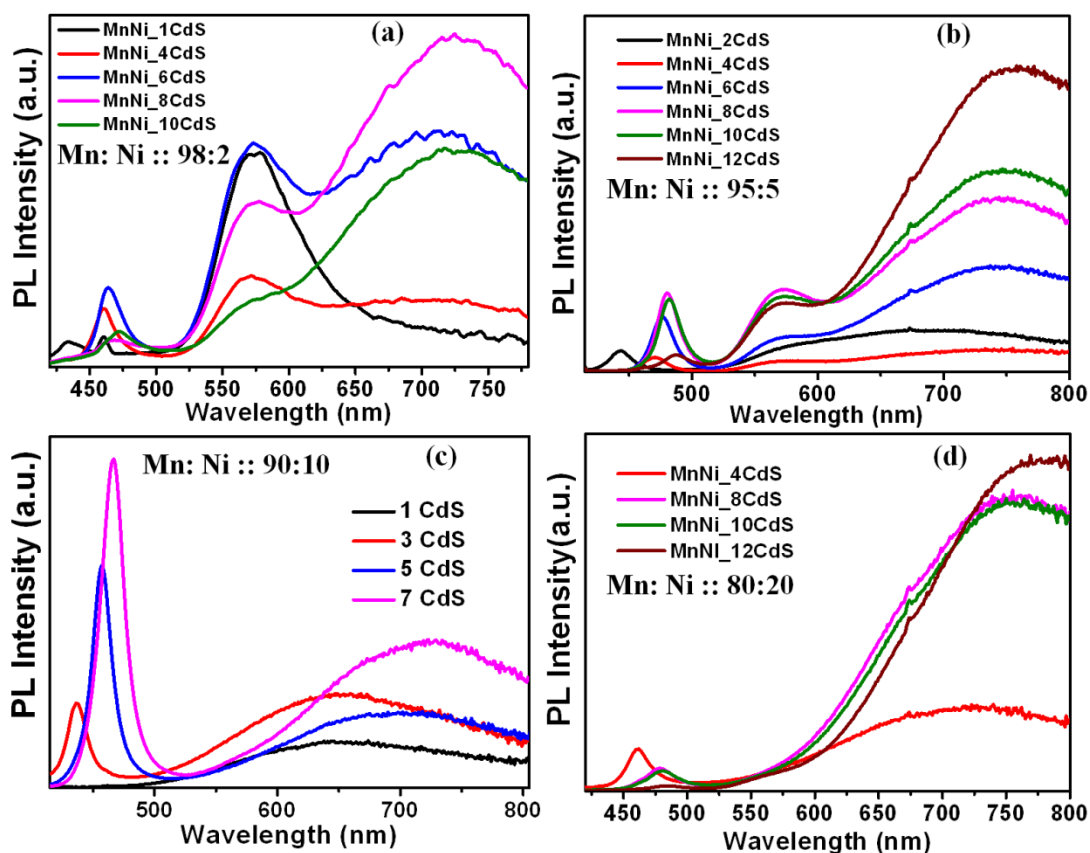


Figure 3.8. shows the steady state emission spectra for different Mn: Ni ratio. (a) Mn: Ni :: 98: 2 (b) Mn: Ni :: 95:5 (c) Mn: Ni :: 90: 10 (d) Mn: Ni :: 80: 20 stoichiometrically.

shows the presence of considerable amount of manganese ions in the nanocrystals, but the emission spectra shows no presence of Mn^{2+} characteristic peak which proves that the electrons at increasing percentages of Ni^{2+} ions in the nanocrystals system decays through the state

introduced by the Ni dopant. As Ni concentration increases, generation of more Ni dopant states takes place which are able to withdraw more electrons from Mn d state. Hence as the Mn:Ni ratio was increased to 80:20, there seems to be no signature of manganese ions in the steady state emission instead the Ni^{2+} emission peak become highly intense. With the increase in shells, the intensity of the Ni dopant peak increases. Figure 3.9. shows the lifetime at 570 nm for different

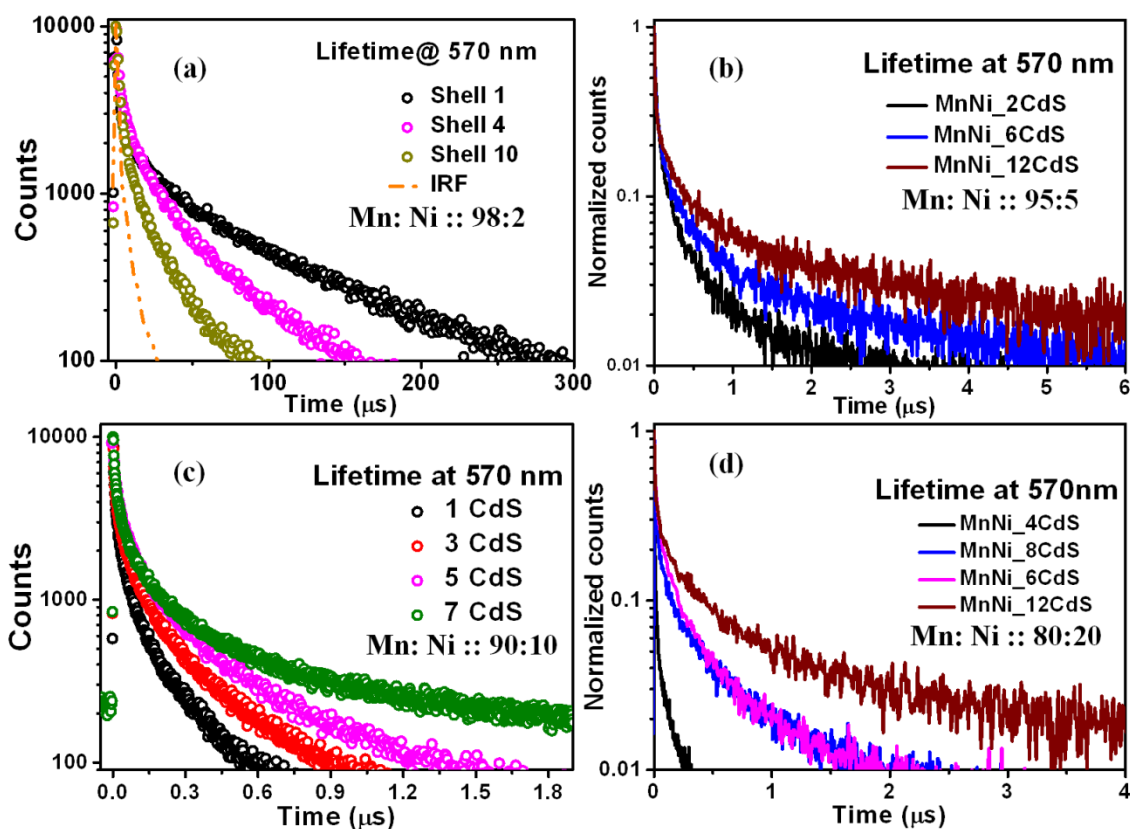


Figure 3.9. shows the time resolved photoluminescence measurements at 570 nm for different Mn: Ni ratio co-doped CdS nanocrystals. (a) Mn: Ni :: 98: 2 (b) Mn: Ni :: 95:5 (c) Mn: Ni :: 90: 10 (d) Mn: Ni :: 80: 20 stoichiometrically.

Mn: Ni ratios for co-doped nanocrystals. As the number of shells increases, there is the increase in the lifetime at 570 nm apart from the case where Ni^{2+} was minimum shown in figure 3.9 (a).

When the Nickel percentage increases, the lifetime of the Mn dopant peak decreases showing there is some kind of contribution coming from the impurity state introduced by Ni^{2+} ions. The Ni dopant emission peak becomes broader with the increase in percentage of nickel showing the increment in the contribution from the Ni impurity state.

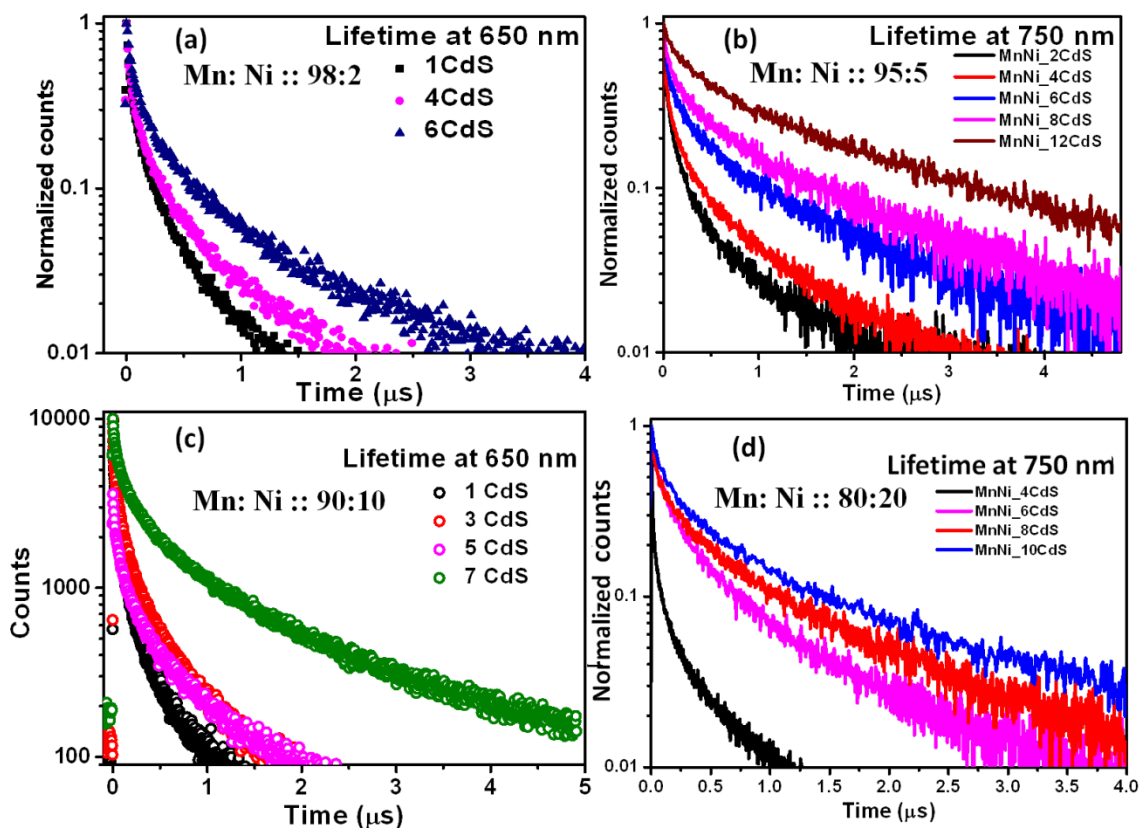


Figure 3.10. shows the time resolved photoluminescence measurements taken at Ni dopant peak for different Mn: Ni ratios for co-doped CdS nanocrystals. (a) Mn: Ni :: 98: 2 (b) Mn: Ni :: 95:5 (c) Mn: Ni :: 90: 10 (d) Mn: Ni :: 80: 20 stoichiometrically.

Figure 3.10 shows the time resolved photoluminescence measurement at Ni dopant peak for different Mn, Ni co-doped nanocrystals. The lifetime studies shows that as the number of CdS shells were grown, the lifetime at the dopant peak increases.

3.6 Future work:

Characterizations performed here show the successful synthesis of the Mn, Ni co-doped nanocrystals using successive ionic layer adsorption and reaction (SILAR) method. Future work will be focused on the study of decay dynamics of these co-doped nanocrystals by time-resolved photoluminescence spectroscopy. As discussed, time resolved spectra shows high Mn lifetime in millisecond (ms) range in Mn doped QDs whereas Ni is has lifetime in microsecond (μ s) range in Ni doped QDs. In co-doped nanocrystals, we want to exploit this difference in lifetime to study the mechanism of Mn and Ni excitation and emission. Thus, thorough analysis of steady state emission and time resolved photoluminescence spectra will be done to explain the decay dynamics and electronic structure of these Mn, Ni co-doped nanocrystals.

3.7 References and notes

- (1) Panda, S. K.; Hickey, S. G.; Demir, H. V.; Eychmaller, A. *Angew. Chem.* **2011**, *123*, 4524-4528.
- (2) Viswanatha, R.; Naveh, D.; Chelikowsky, J. R.; Kronik, L.; Sarma, D. D. *J. Phys. Chem. Lett.* **2011**, *3*, 2009-2014.
- (3) Jana, S.; Srivastava, B. B.; Pradhan, N. *J. Phys. Chem. Lett.* **2011**, *2*, 1747-1752.
- (4) Archer, P. I.; Santangelo, S. A.; Gamelin, D. R. *Nano Lett.* **2007**, *7*, 1037-1043.
- (5) Bhargava, R. N.; Gallagher, D.; Hong, X.; Nurmikko, A. *Phys. Rev. Lett.* **1994**, *72*, 416.
- (6) Norris, D. J.; Yao, N.; Charnock, F. T.; Kennedy, T. A. *Nano Lett.* **2001**, *1*, 3-7.
- (7) Nag, A.; Sapra, S.; Nagamani, C.; Sharma, A.; Pradhan, N.; Bhat, S. V.; Sarma, D. D. *Chem. Mater.* **2007**, *19*, 3252-3259.
- (8) Stowell, C. A.; Wiacek, R. J.; Saunders, A. E.; Korgel, B. A. *Nano Lett.* **2003**, *3*, 1441-1447.
- (9) Somaskandan, K.; Tsoi, G. M.; Wenger, L. E.; Brock, S. L. *Chem. Mater.* **2005**, *17*, 1190-1198.
- (10) Manna, G.; Jana, S.; Bose, R.; Pradhan, N. *J. Phys. Chem. Lett.*, *3*, 2528-2534.
- (11) Pradhan, N.; Peng, X. *J. Am. Chem. Soc.* **2007**, *129*, 3339-3347.
- (12) Jana, S.; Srivastava, B. B.; Jana, S.; Bose, R.; Pradhan, N. *J. Phys. Chem. Lett.* **2012**, *3*, 2535-2540.
- (13) Srivastava, B. B.; Jana, S.; Pradhan, N. *J. Am. Chem. Soc.* **2011**, *133*, 1007-1015.
- (14) Grandhi, G. K.; Tomar, R.; Viswanatha, R. *ACS Nano* **2012**, *6*, 9751-9763.
- (15) Sankapal, B. R.; Mane, R. S.; Lokhande, C. D. *Mater. Res. Bull.* **2000**, *35*, 177-184.

- (16) Li, J. J.; Wang, Y. A.; Guo, W.; Keay, J. C.; Mishima, T. D.; Johnson, M. B.; Peng, X. *J. Am. Chem. Soc.* **2003**, *125*, 12567-12575.
- (17) Reiss, P.; Protiere, M.; Li, L. *Small* **2009**, *5*, 154-168.
- (18) Yu, W. W.; Peng, X. *Angew. Chem. Int. Ed.* **2002**, *41*, 2368-2371.

JOHN WILEY AND SONS LICENSE
TERMS AND CONDITIONS

Mar 29, 2015

This Agreement between KUSHAGRA GAHLOT ("You") and John Wiley and Sons ("John Wiley and Sons") consists of your license details and the terms and conditions provided by John Wiley and Sons and Copyright Clearance Center.

License Number	3597341100134
License date	Mar 27, 2015
Licensed Content Publisher	John Wiley and Sons
Licensed Content Publication	Advanced Functional Materials
Licensed Content Title	Mn ²⁺ -Doped CdSe Quantum Dots: New Inorganic Materials for Spin-Electronics and Spin-Photonics
Licensed Content Author	Rémi Beaulac, Paul I. Archer, Stefan T. Ochsenbein, Daniel R. Gamelin
Licensed Content Date	Nov 25, 2008
Pages	19
Type of use	Dissertation/Thesis
Requestor type	Author of this Wiley article
Format	Print and electronic
Portion	Figure/table
Number of figures/tables	2
Original Wiley figure/table number(s)	Figure 1 (a), Figure 1 (b)
Will you be translating?	No
Title of your thesis / dissertation	Study of Mn d-d emission mechanisms in II-VI semiconductor nanocrystals
Expected completion date	Mar 2015
Expected size (number of pages)	80
Requestor Location	KUSHAGRA GAHLOT JNCASR STUDENTS' RESIDENCE ROOM NO. 54 JAKKUR BANGALORE, India 560064 Attn: KUSHAGRA GAHLOT
Billing Type	Invoice
Billing Address	KUSHAGRA GAHLOT

JNCASR STUDENTS' RESIDENCE
ROOM NO. 54
JAKKUR
BANGALORE, India 560064
Attn: KUSHAGRA GAHLOT
0.00 USD

Total